Low Dimensional Freestanding Semiconductors for Flexible Optoelectronics: Materials, Synthesis, Process, and Applications

Jung-Hun Seo[1,*], Edward Swinnich[1], Yi-Yu Zhang[2], Munho Kim[2,*]

[1]Department of Materials Design and Innovation, University at Buffalo, The State University of New York, Buffalo, NY USA 14260

[2]School of Electrical and Electronic Engineering, Nanyang Technological University, 50 Nanyang Avenue, 639798 Singapore, Singapore.

[*]Author to whom correspondence should be addressed; email: junghuns@buffalo.edu and munho.kim@ntu.edu.sg

Abstract

In this review, the primary focus is the recent advances in the development of freestanding inorganic crystalline semiconductors and their manipulation technology for flexible optoelectronic applications. We firstly cover the details of the growth and processing techniques of freestanding inorganic crystalline semiconductors in various dimensions and their material property under strain condition. Finally, fabrication processes and opto-electrical properties of flexible optoelectronics are introduced. Future research directions are also discussed, including further enhancement of device performance, building more types of optoelectronic devices on flexible substrates, and process integration for the advanced optoelectronic circuits and systems.

Introduction

Optoelectronic devices such as photosensors, light-emitting devices, and photovoltaics are essential components in numerous modern applications: digital imaging, displays, motion detectors, and energy convergence systems [1]. Most of the optoelectronics use the quantum mechanical effect of light such as carrier confinement and carrier generation/recombination in semiconductors including a wide range of epitaxially grown inorganic semiconductors such as Si, Ge, III-V, and III-nitride [2]. Because these semiconductors are grown from their own wafer substrates, conventional optoelectronic devices and their applications must accommodate thick, rigid, fragile, and planar form factors. On the other hand, flexible optoelectronics are different from traditional optoelectronics in that devices can be built on flexible substrates, permitting their use in unconventionally shaped optoelectronic applications [3,4]. This major advantage allows the development of flexible optoelectronics that can revolutionize day-to-day life, unshackling the restrictions of a rigid and planar design. For example, a conventional charge-coupled device in a digital camera requires a series of lenses to collimate the beam path before the light hits the flat photosensor. In contrast, most animal eye systems have curved retinas that eliminate or minimize beam correction [5-7], thus offering much simpler and efficient sensing structures. Also, a flexible and rollable display can offer compact and mechanically durable displays, ideal for compact and lightweight mobile communications [8]. Additionally, flexible optoelectronic devices can be bent, twisted, and stretched because they are mechanically flexible, stable, and durable [4], which offer a great degree of freedom in re-designing optoelectronic applications wherein uneven surfaces such as skin, organs, or moving parts such as joints or wheels can be seamlessly covered [5]. Therefore, advances in flexible optoelectronics will ignite various wearable, attachable, and implantable bioelectronics that are not possible with conventional technology [9,10].

To build flexible optoelectronics, as depicted in Figure 1, two research efforts must be simultaneously pursued to develop: 1) freestanding low-dimensional semiconductors and 2) unconventional micro- and nano-fabrication.

Firstly, freestanding low-dimensional semiconductors include the freestanding form of conventionally grown nanomaterials or epitaxially grown semiconductors that can self-sustain without support from substrates. These freestanding semiconductors exist as one-, two-, and quasi-two-dimensional objects such as nanowires (NWs) [11,12], nanobelts [13,14], atomically thin sheets [15-17], and nanomembranes (NMs) [18]. These are typically synthesized on rigid host substrates using various conventional growth methods: chemical vapor deposition (CVD), molecular-beam epitaxy (MBE), and metal organic chemical vapor deposition (MOCVD). Secondly, after growth, the nanostructures are separated from the host substrates and then converted into freestanding forms using various conversion approaches. Rogers et al. have described the details of various separation routes [18]. These separation processes make the conventional semiconductors unique as freestanding forms that are highly flexible and able to be relocated to any new and foreign substrates. It should be noted that the separation and relocation processes are as crucial as the material synthesis itself. As shown in Figure 1, the most popular methods for handling the freestanding semiconductors are (1) dispersion and spraying [19,20], (2) growth directly on metallic foils [21,22], and (3) micro-transfer printing [22]. The advantage of these approaches lies in the additive process, which reduces fabrication costs and offers great freedom when designing atomic- or nano-scale semiconductor structures using a batch-wise process. Other attractive features of this technology include reduced material waste and scalability to large-area manufacturing.

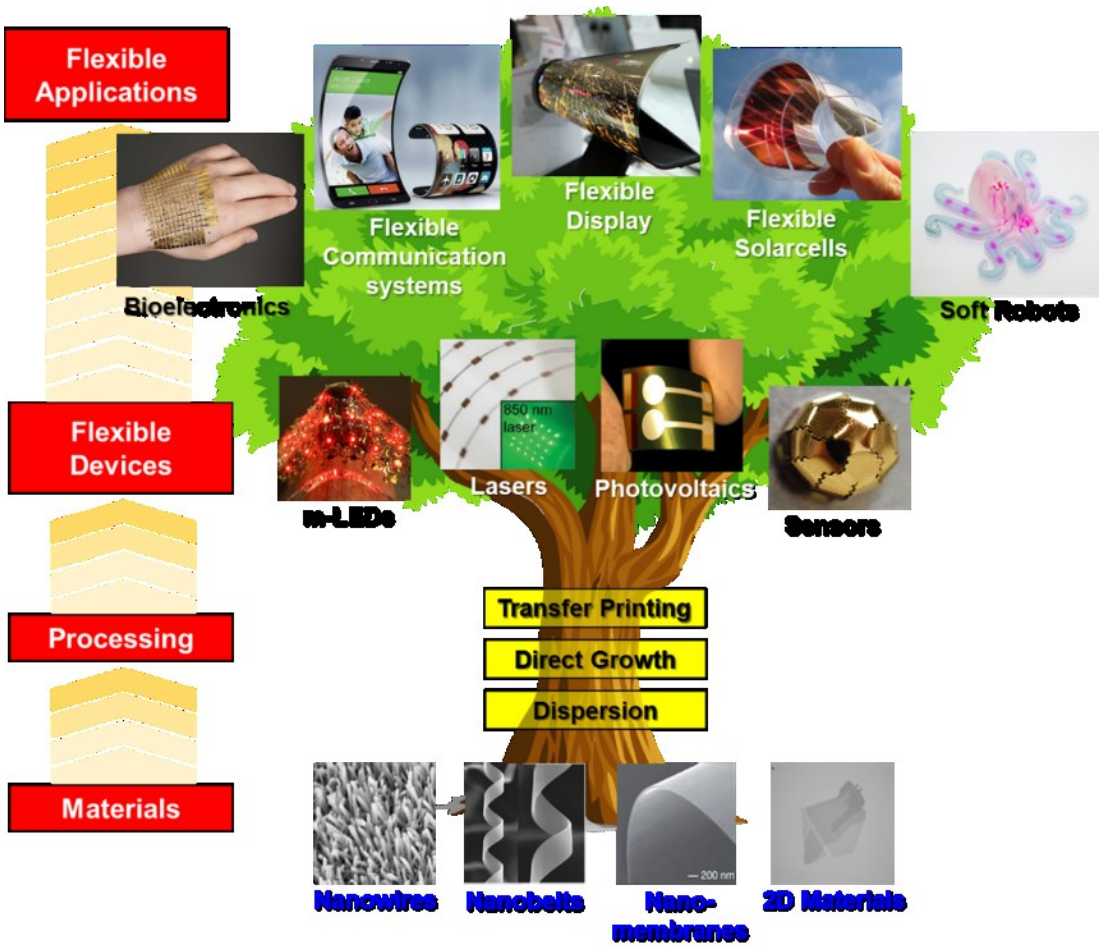

Figure 1. An illustration to show the outline of this review paper, covering various freestanding nanomaterials and processing technologies for flexible optoelectronics.

In this review, as illustrated in Figure 1, the focus is primarily on recent advances in the development of freestanding inorganic crystalline semiconductors and the associated manipulation technology for flexible optoelectronic applications. After describing the details of the growth and the process of freestanding inorganic crystalline semiconductors in various dimensions (one-dimensional semiconductors such as Si-, GaAs-, ZnO-, and GaN NWs, two-dimensional semiconductors such as graphene and MoS_2, and quasi-two-dimensional semiconductors such as perovskite, PbI_2 NMs, In_2Se_3 NMs, ZnS NMs, Ge NMs, III-V NMs, III-nitride NMs, and ZnO NMs), their material properties under strain will be presented. Finally, fabrication processes and

the opto-electrical properties of flexible optoelectronics such as flexible photosensors, lighting devices, and photovoltaics will be introduced.

1. Materials Synthesis

1.1. Freestanding 1-dimensional nanowire semiconductors

Semiconductor NWs are 1D nanostructures with their diameters of the order of a nanometer. Quantum confinement in the NWs has been of great interest because the dimension is either comparable to or smaller than Bohr radius of materials [23]. An array of the inorganic semiconductor NWs provides an excellent platform for various electronic and optoelectronic devices demonstrating carrier mobility up to 21,000 $cm^2/(V \cdot s)$ and excellent light absorption capability [24]. In addition, they are inherently flexible due to significantly reduced rigidity. This offers promises for high performance flexible and stretchable electronic and optoelectronic applications which can exceed the performance of organic or amorphous semiconductor-based flexible devices. Many different types of the NWs such as core-shell Ge/Si NWs, InAs NWs, and GaN NWs have been reported [25-27]. The synthesis of the NWs has been realized by both bottom-up and top-down approaches via epitaxial growth and etching, respectively [24]. These NWs can be prepared with high throughput and controllable material properties including shape, size, and doping concentration. However, the synthesized NWs are not directly applicable for flexible applications because they are still bound to its original substrates. Therefore, researchers have endeavored to develop methods to form freestanding NWs by releasing them from donor substrates without sacrificing original material properties.

1.1.1 The direct growth of single crystalline GaN NWs on flexible substrate:

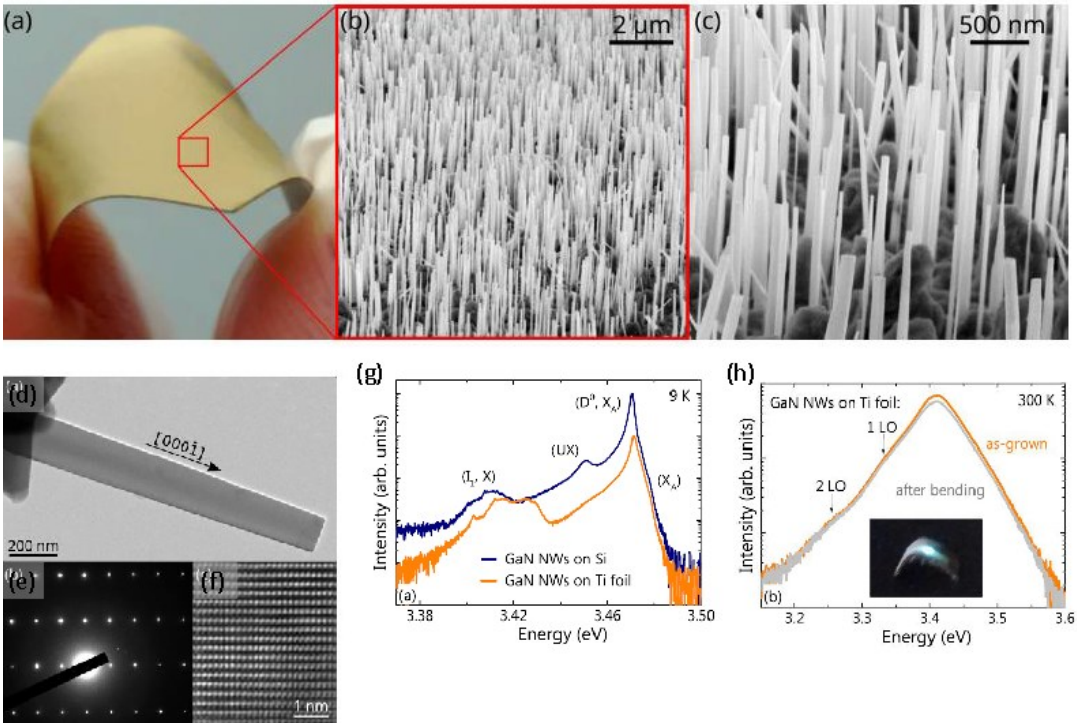

Figure 2. (a) Photograph of the Ti foil after NW growth demonstrating a high degree of flexibility. [(b) and (c)] Scanning electron micrographs of the GaN NW ensemble grown on the Ti foil taken in bird's eye view with (b) low and (c) high magnification. (d) Bright-field transmission electron micrograph of a single representative GaN NW grown on the Ti foil. (e) SAED pattern of the NW shown in (d). (f) Lattice image of a section of the NW shown in (d) taken along the <1100> zone axis. (g) Low temperature (9 K) and (h) Room-temperature PL spectra of the GaN NW ensemble grown on the Ti foil. [31].

The synthesis of single crystalline NWs has been well developed by epitaxial growth techniques using MBE and metal organic chemical vapor deposition [28,29]. However, the creation of freestanding single crystalline NWs has technical issues such as the absence of releasing techniques. The most effective method is to grow NWs on top of flexible substrates which eliminate the need for releasing process [30]. However, the direct growth of inorganic NWs on flexible substrates is limited by interfacial reactions between grown NWs and metallic flexible substrates and low melting temperature of organic flexible substrates.

Calabrese et al. used the plasma-assisted MBE (PA-MBE) technique to synthesize single crystalline GaN NWs on a flexible Ti foil [31]. Metal foil is regarded as an attractive substrate because it is not only flexible but also exhibits good electrical and thermal properties. The polycrystalline Ti foil was out-gassed and nitridated at 750 ˚C and 1000 ˚C for 20 min, respectively, in the preparation chamber of the MBE prior to NW growth. The growth of GaN NWs was performed with Ga and N fluxes at 730 ˚C for 4 h. Figure 2(a) shows a photograph of the bent Ti foil after GaN NW growth. Figure 2(b) and (c) show scanning electron microscope (SEM) images of vertically aligned GaN NWs. Large surface roughness between the NWs was observed due to interfacial reactions between Ga and Ti at non-nitridated regions of the substrate. Statistical study indicates that the average values and standard deviation of the NW length, diameter, and density are (11.4 ± 0.37) μm, (70 ± 40) nm, and 8.2×10^7 cm^{-2}, respectively. It is noted that the density of misoriented NWs is low, which will avoid degradation of the final performance of devices built on these GaN NWs because the misoriented NWs will be hardly contacted during fabrication of the devices. Morphology and degree of crystallinity of twenty individual GaN NWs were characterized by transmission electron microscope (TEM). Figure 2(d) shows an exemplary bright-field TEM image of a single GaN NW. No basal-plane stacking faults were observed from structurally uniform dislocation-free NW. The selected area electron diffraction (SAED) pattern of the whole NW confirms the single crystallinity in the wurtzite form (Figure 2(e)). The high-resolution TEM reveals the lattice of the wurtzite structure (Figure 2(f)), further confirming the structural perfection of the GaN NWs grown on the Ti foil, which is comparable to that of uncoalesced NWs grown on Si(111) substrates. The structural perfection of the GaN NWs was additionally investigated by continuous-wave-photoluminescence (CW-PL) spectroscopy. Figure 2(g) shows a near-band-edge low-temperature PL spectrum taken at 9 K. The

PL spectrum of a standard GaN NW grown on Si(111) at 835 ˚C was included for comparison. The spectra indicates the dominant recombination of excitons bound to neutral O donors [(D^0, X_A]] at 3.471 eV, showing that GaN NWs are free of homogeneous strain [32]. The full-width-at-half-maximum (FWHM) of this transition of the GaN NW grown on Ti foil and Si(111) is 2.2 and 1.5 meV, respectively. The effect of bending on the luminescence of the NW was characterized by room-temperature PL. Figure 2(h) shows the comparison of the near-band-edge PL spectra prior to and after bending the foil under a positive radius of curvature of 4 mm. Inset shows a photograph of the bent foil. Identical PL spectra were obtained with the free A exciton transition centered at 3.41 eV with an FWHM of 64 meV before and after bending. The self-assembled growth of single crystalline, well-oriented, and uncoalesced N-polar wurtzite GaN NWs on a flexible Ti foil can offer the pathway for the realization of flexible GaN NW-based electronic and optoelectronic devices.

1.1.2 Formation of NWs by etching followed by lift-off and transfer: Si NWs by metal-assisted chemical etching

Another method to fabricate NWs is a direct dry or wet etching of bulk materials. Advantages of this method include an easy control of dimension and morphology of the NWs. Conventional or deep RIE has employed to fabricate various semiconductor NWs. Recently, metal-assisted chemical etching (MacEtch) have drawn much interest as an alternative top-down technique to form various semiconductor nanostructures such as vias, pillars, NWs, pyramids, fins, and nano-groves [33-37]. The typical Si MacEtch starts by depositing the noble metal catalyst on the substrate. The catalyst can be patterned into any arbitrary shapes. Then, the sample is immersed in the solution mixture of hydrofluoric acid (HF) and hydrogen peroxide (H_2O_2) to selectively

oxidize and dissolve the Si localized under the catalyst. Detailed mechanism and device application of the MacEtch can be found elsewhere [38]. Weisse et al. recently reported a fabrication and characterization of flexible vertical Si NWs [39]. MacEtch and PDMS-assisted technique were developed to form the Si NWs and lift-off and transfer them on flexible substrates, respectively.

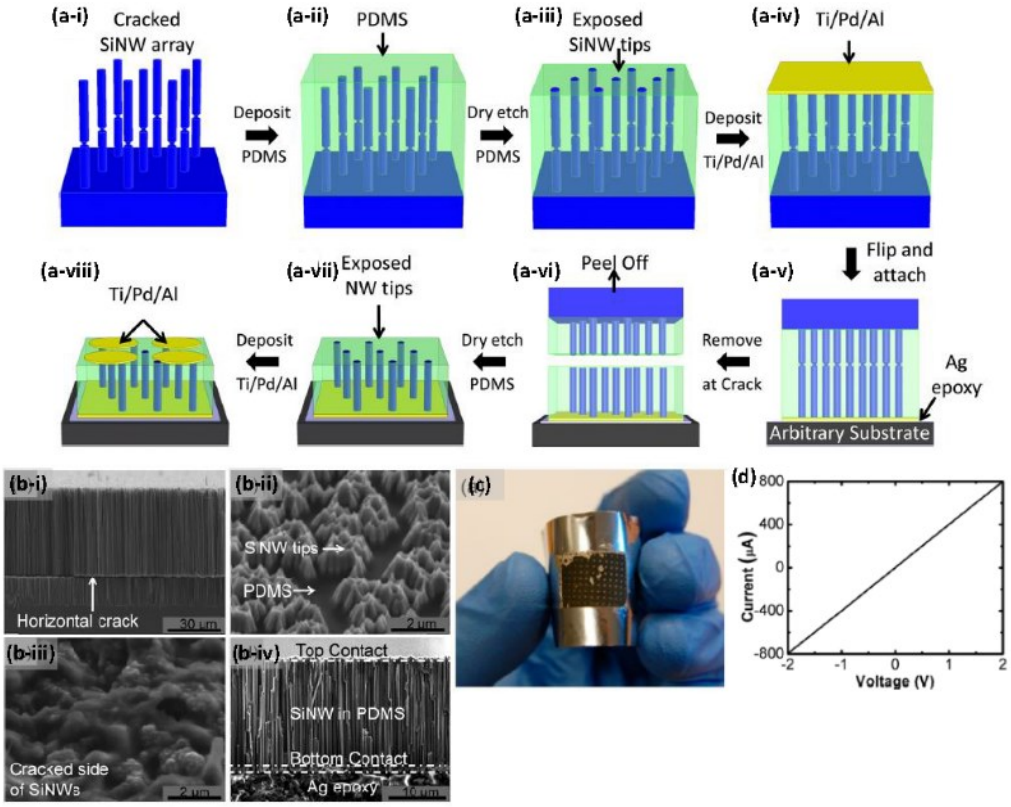

Figure 3. (a) Schematic of the fabrication procedure for vertical Si NW array electronic devices on non-Si-based substrates with V-TPM. (b) SEM images of various aspects of Si NW array. (c) Optical images of vertical nonporous Si NW devices fabricated on a stainless steel foil. (d) I–V curve of a typical vertical nonporous Si NW device. [39].

Figure 3 shows a schematic process flow of vertical Si NW array electronic devices on arbitrary substrates. The process begins by a formation of cracked vertical Si NWs by using Ag-assisted chemical etching of p-type Si wafer (Figure 3(a-i)). The horizontal crack across the Si NWs was created by inserting a water soaking step between two consecutive etching steps. Formation of the horizontal crack was attributed to the delamination and redistribution of Ag in

water. The samples were filled with diluted PDMS by spin coating (Figure 3(a-ii)) and further dry etched by RIE with CHF_3:O_2 gas mixture (Figure 3(a-iii)) to expose the Si NW tips. Then, metal contacts (Ti/Pd/Al: 5/200/500 nm) were deposited on the exposed NW tips by e-beam evaporator (Figure 3(a-iv))) and followed by flip-transfer on Ag epoxy coated arbitrary substrates (Figure 3(a-v)). The Si NWs were detached from Si substrates at the horizontal crack lines with the assistance of gentle shear force (Figure 3(a-vi,vii)). Finally, the same metal contacts were deposited on the other side of the NW tips (Figure 5(a-viii)). Figure 3(b) and (c) show SEM images of the NW arrays at each stage of the fabrication and an optical image of vertical Si NW devices on a stainless steel foil. I-V characteristic of the devices was measured, demonstrating the formation of ohmic contact to the Si NW tips on both sides of the array (Figure 3(d)).

1.2. 2-dimensional material

In the past decade, 2D atomic crystals have gained tremendous interests in the field of electronic and optoelectronic devices due to their intriguing physics and various applications [40-41]. The 2D atomic crystals are atomically thin and layered crystalline solids with covalent and van der Waals bonding thus have unique electro-mechanical properties under the bending conditions [42-43]. Various 2D materials mostly studied in the past years include graphene, and transition metal dichalcogenides (TMDs) [44-45]. It is important to realize large size defect-free monolayer to take advantage of superior properties for device applications. In this section, we present the recent progress of monolayer graphene, molybdenum disulfide (MoS_2), and its integration towards flexible optoelectronic devices.

1.2.1 Monolayer graphene

Graphene is a highly promising material for photo-detection across the broadband wavelength regions from visible to infrared (IR) regions due to its strong absorption per unit mass [46]. It has become a core material for various types of photodetectors (i.e., metal-graphene-metal and p-n junction) since the first graphene-based photodetectors, which operated at a wavelength range from 300 nm to 6 μm [47]. In addition, constant photoresponse was observed from the metal-graphene-metal photodetectors under optical modulations up to 40 GHz [48].

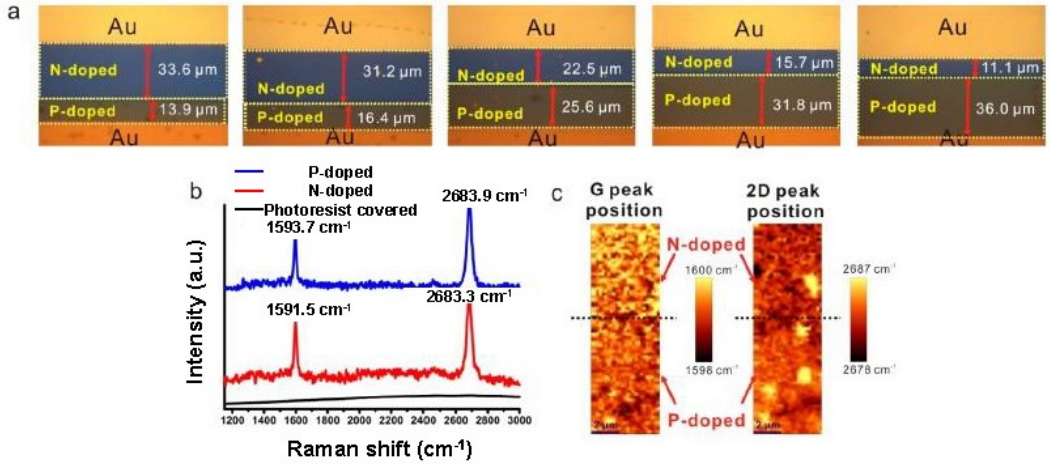

Figure 4. (a) Optical images of the graphene P-N junctions, highlighting both the P- and N-regions. (b) Raman spectra of undoped (P-type, blue) and o-MeO-DMBI-I− (6 nm)-doped (red) and photoresist-covered (black) CVD-graphene. (c) Maps of G and 2D peak position in the junction region. [49].

Liu et al. reported the first flexible and transparent graphene IR photodetectors based on p-n junctions [49]. Firstly, the monolayer graphene was grown on Cu foil via chemical vapor deposition (CVD). The CVD-grown graphene was transferred on a Si substrate by Poly(methyl methacrylate) (PMMA)-assisted wet transfer method. The Si substrate consisted of a 300 nm SiO_2, capped with a 20 nm thermally cross-linked divinyltetramethyldisiloxane bis-(benzocyclobutene) (BCB). The BCB layer was intended to provide an effect surface passivation for hole and electron traps. Then, a layer of photoresist was spin-coated on the graphene and Au electrodes were patterned. The compound 2-(2-methoxyphenyl)-1,3-dimethyl-2,3-dihydro-1*H*-benzoimidazole (*o*-

MeO-DMBI) was used as a strong n-type dopant for CVD-grown graphene [50]. The *o*-MeO-DMBI film was deposited on the open area by the thermal evaporation. It is well known that undoped CVD graphene is highly p-type doped. Therefore, the graphene covered with *o*-MeO-DMBI film were n-type doped and p-n junction was formed in the graphene. This method enables to selectively form doping areas by controlling the exposed area by photolithography.

Figure 4(a) shows optical images of the graphene p-n junctions where p-type region was covered by the photoresist. Raman spectroscopy was performed on the graphene to confirm that the photoresist effectively blocks the covered region (i.e., p-type graphene) from n-type doping by the *o*-MeO-DMBI film. Figure 4(b) shows Raman spectra measured on the p-, n-doped, and covered graphene. The clear G and 2D peaks were observed from both p- and n-doped graphene while no peaks were detected from the photoresist covered graphene. The G peak of both p-doped (i.e., undoped) and n-doped graphene shifted to a larger wavenumber, indicating that the transferred graphene was doped. In addition, Raman mapping was carried out in the adjacent 5 × 15 μm^2 p-type and n-doped regions, using 0.2 μm as a step increment (Figure 4(c)) to characterize the average level of doping density.

1.2.2 Monolayer MoS_2

Monolayer MoS_2 has intrigued much research interests as it has a direct bandgap energy of 1.9 eV [45]. Atomically thin, uniform, and large-size MoS_2 can be synthesized by one-step CVD technique. In addition, it is regarded as an excellent material for flexible device applications due to strong mechanical durability under bent conditions. However, functional layers required for MoS_2-based devices still requires the use of inorganic materials formed by atomic layer deposition (ALD) and thermal or e-beam evaporation, which are not compatible with large-size flexible

platforms. Electrical characteristics of MoS_2 can be degraded by processing steps such as photolithography.

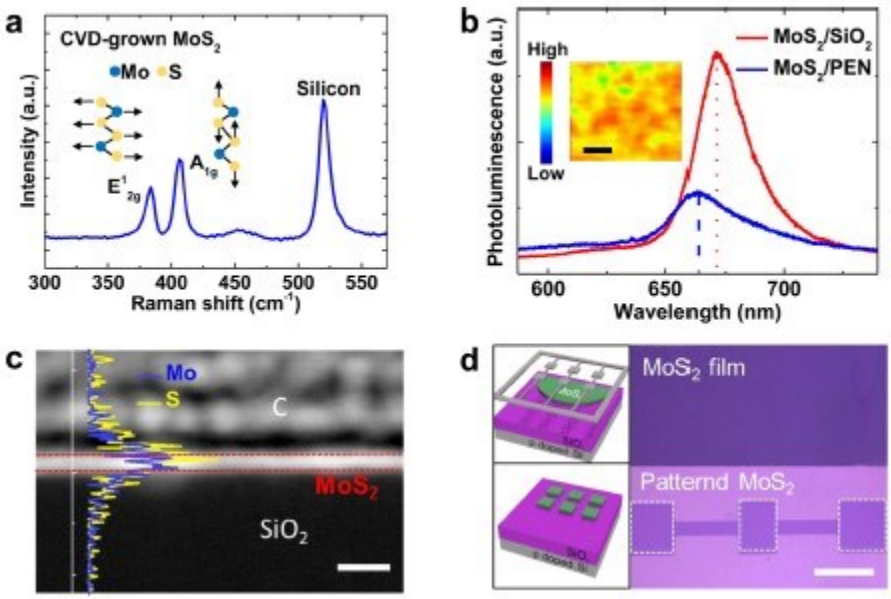

Figure 5. (a) Raman spectrum of a CVD-synthesized monolayer MoS2 film on a SiO_2/Si substrate. (b) PL spectra of CVD-synthesized monolayer MoS_2 films on SiO_2/Si and PEN substrates. The inset shows a PL intensity mapping at 670 nm (=1.85 eV). Scale bar is 5 μm. (c) EDS data of Mo (blue line) and S (yellow line) and a cross-sectional STEM image of a CVD-synthesized MoS_2 film on a SiO_2/Si substrate. Scale bar is 5 nm. (d) Optical images of a CVD-synthesized MoS_2 channel before (top) and after (bottom) selective patterning processes. Scale bar is 400 μm. [51].

Kim et al. addressed these challenges by using a drop-on-demand inkjet-printing technology to fabricate all organic and MoS_2 based flexible and transparent phototransistor arrays [51]. Firstly, a large-size monolayer MoS_2 film was synthesized by MoO_3 and sulfur (S) powders and transferred on SiO_2/Si substrates. Then, patterned CVD-grown MoS_2 film was transferred on a polyethylene-naphthalate (PEN) substrate via the PMMA-assisted transfer method. The material property of the MoS_2 film was characterized by various methods such as Raman spectroscopy, PL, TEM, and XPS. It was confirmed that the MoS_2 is uniformly grown monolayer based on the Raman peak difference (~20.7 cm^{-1}) between in-plane (E_{2g}) and out-of-plane (A_{1g}) (Figure 5(a)) and a distinct PL peak A (~670 nm) (Figure 5(b)). The PL signal of the MoS_2 on the PEN substrate was

blue-shifted by a slight tensile strain induced in the MoS_2 due to the difference in thermal expansion coefficients of the MoS_2 and SiO_2/Si. Inset in Figure 5(b) shows a PL mapping scanned over 20 × 20 μm^2, indicating the MoS_2 film has a uniform bandgap energy of 1.85 eV. TEM and energy dispersive X-ray spectroscopy (EDS) characterizations further supported that the monolayer MoS_2 was grown well (Figure 5(c)). Patterning of the MoS_2 film is a critical step to fabricate phototransistor arrays. It is noted that the CVD-grown monolayer MoS_2 film typically has a dark violet color on 270 nm SiO_2. The color difference of the patterned MoS_2 film indicated that the film was selectively etched by oxygen plasma (Figure 5(d)).

1.3. Quasi-2D nanomembranes (NMs)

Transferrable inorganic semiconductor NMs are one of the emerging materials in realizing unconventional electronic and optoelectronic devices [52]. Representative NMs include group IV (Si and Ge), group III-V (GaAs, InP, and InAs, etc.), and wide band-gap (GaN and 4H-SiC) semiconductors [53-60]. Therefore, it is very important to secure their original substrates for supplying high quality NMs. Newly engineered substrates consisting of a top semiconductor layer, insulating sacrificial layer, and handling substrate have attracted much attention as a source material for the transferrable semiconductor NMs. Among various fabrication techniques, Smart-Cut^{TM} is the most popular method because excellent material qualities can be obtained due to the single crystallinity of the top layer [61]. A wide range of X on insulator (X-OI) substrates have been fabricated, including Si on insulator (SOI) [61], Germanium on insulator (GeOI) [57], and 4H-SiC on insulator (4H-SiCOI) [60]. These substrates serve as a donor material for transferrable semiconductor NMs [58,62]. Transfer printing of semiconductor NMs is a unique process which enables delamination of single crystalline NMs from their native substrates (i.e., SOI and GeOI)

and its subsequent transfer onto non-native substrates [63]. The delamination of NMs is realized by selectively etching underlying sacrificial layers.

The abovementioned semiconductor NMs have been actively studied to enhance the performance of various electronic/optoelectronic devices such as reflectors [55-55], photodetectors [64-66], light emitting diodes [67-69], and transistors [56,70]. They are either becoming the main body of the devices or adding additional functionalities as a key enabler for the enhanced performance. In this section, we will summarize the recent development and process of the various semiconductor NMs in a field of flexible optoelectronic devices. Detailed fabrication methods and characterizations of the materials will be discussed.

1.3.1 Ge NMs

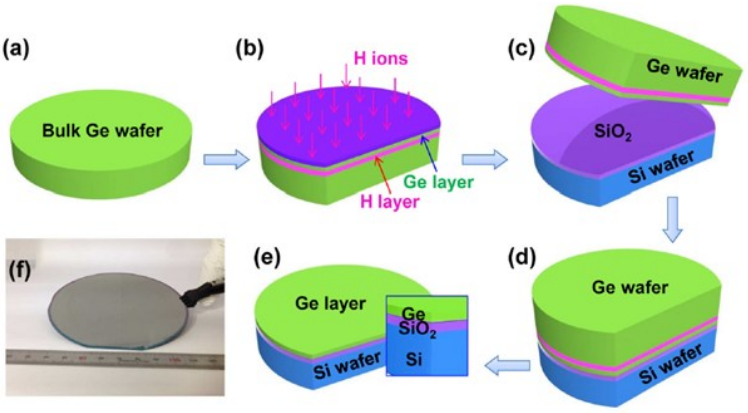

Figure 6. A schematic process flow of the fabrication of GeOI wafer: (a) Cleaning a bulk Ge wafer. (b) Depositing a 100 nm thick PECVD SiO_2 layer on top of the Ge wafer followed by hydrogen implantation. (c) Wafer bonding to thermally oxidized Si handling wafer. (d) Annealing the bonded wafers for splitting Ge layers by hydrogen exfoliation. [55].

Germanium (Ge) is a group IV semiconductor with a bandgap energy of 0.66 eV. Due to a high absorption coefficient, Ge has been actively utilized as a light absorption material in a near infrared (NIR) region [35]. The absorption coefficient remains high and it sharply drops when the wavelength exceeds 1.55 μm. In addition, Ge has gained much interests as a candidate for CMOS

compatible light emitter as its indirect band structure can be modified to direct under tensile strain [71]. A 4 inch GeOI, a source material, was fabricated by Smart-Cut technique [55]. Figure 6(a-e) show the fabrication process of the GeOI wafer. In this process, unintentionally doped (resistivity > 40 Ω-cm) bulk Ge wafer was used. 100 nm PECVD SiO_2 layer was deposited onto Ge wafer as a screen oxide to obtain a uniform ion implantation profile. The Ge wafer coated with the oxide was implanted by H^+ ions with a dose of 1×10^{17} cm^{-2} and an energy of 100 keV (Figure 6(b)). The hydrogen implantation profile was carefully designed to be located at 700 nm from a Ge surface to obtain a Ge layer with a 400 nm thickness. Then, 200 nm SiO_2 was thermally grown onto a handling Si substrate as the buried oxide (BOX) to fabricate the final structure of GeOI. The SiO_2 on the Ge wafer was removed by HF (49%) prior to bonding. The oxygen plasma was used to enhance a bonding strength between Ge and oxidized Si substrate. The wafer bonding process was conducted using wafer bonder (EV 801) in a vacuum condition of 7×10^{-5} mbar (Figure 6(c,d)). Two step low temperature annealing at 200 and 250℃ was performed in a nitrogen-filled oven to obtain the complete separation of Ge layer from the Ge bulk substrate via a nucleation of hydrogen platelets (Figure 6(e)). Consequently, ~ 700 nm Ge layer was transferred onto SiO_2/Si handling wafers. Chemical and mechanical polishing (CMP) was performed to remove implantation defected Ge regions. Figure 6(f) exhibits an optical image of the fabricated 4-inch GeOI wafer. No visible voids were observed across the entire Ge surface. Figure 6(g-i) shows an SEM image of a vertical structure of the GeOI wafers. The measured thicknesses of Ge and BOX layer were measured to be 400 and 200 nm, respectively. There values corresponded well with a target thickness of each layer. It is crucial to identify crystallinity and residual strain of the Ge layer in the fabricated GeOI wafer since the thermal annealing process was conducted with a high pressure.

1.3.2 GaN NMs

Both wide bandgap and thermal stability of GaN can make it an ideal material choice for various applications such as high-power and high temperature field-effect transistors (FETs), blue light-emitting diodes, and lasers [72]. Due to its excellent material properties, GaN has become an interesting material toward large area flexible devices and circuits. In general, freestanding GaN thin films have been realized by laser lift-off and direct substrate removal from GaN grown on sapphire and GaN on Si substrates, respectively. However, a material quality of GaN epilayers grown in Si is not superior due to mismatch of lattice and thermal expansion of GaN and Si.

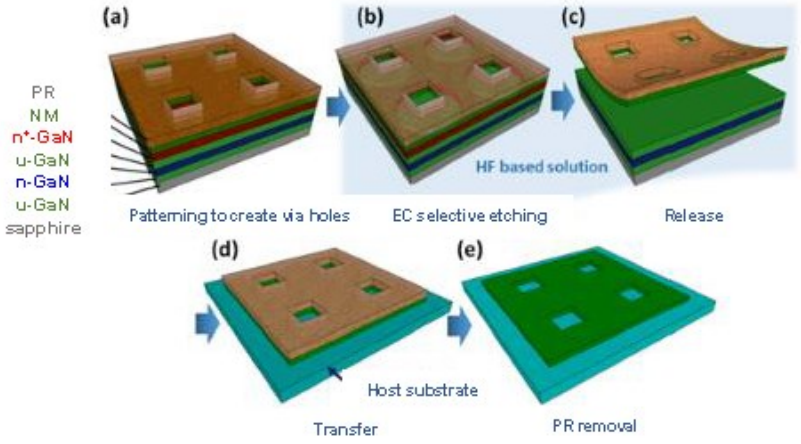

Figure 7. Process flow of preparing III−N NMs. (a) Lithography and etching to expose sidewalls of sacrificial layers. (b) Electrochemical selective lateral etching of the heavily doped GaN sacrificial layer to undercut the NM. (c) Separation of NMs with photoresist (PR) in hydrofluoric acid based solution. (d) Extraction and anchoring of NM (with PR) to the target wafer. (e) Removal of PR by wet or dry cleaning after large-area NM has adhered to the host. [73].

Recently, Park et al. obtained high quality GaN NMs from GaN grown on sapphire substrates via a conductive selective electrochemical (EC) etching of highly doped GaN layers [73]. Figure 7(a-e) shows a schematic of process flows where it begins from epitaxial growth of GaN stack layers on sapphire via MOCVD. An undoped GaN was firstly grown, followed by growth of moderately n-doped layer (thickness: 3.5 μm, doping concentration: 1×10^{18} cm^{-3}) to

improve lateral current flow. This n-type layer is protected by another undoped GaN (thickness: 500 nm). Highly doped GaN layer with a doping concentration of 1.2×10^{19} /cm^3 (the red layer of Figure 7(a)) was subsequently grown as a sacrificial layer. The III-N NM device layers with a thickness of 90 – 300 nm were grown to from either GaN or GaN/InGaN heterostructures. The standard photolithography and RIE were performed to expose the sacrificial layer. The n^+-GaN sacrificial layer was selectively etched due to a high etching rate under the EC etching. Top GaN NMs were released and then transfer-printed via dry or wet procedures (Figure 7(d)). It is noted that the distance between etching vias can be adjusted to 25 - 100 μm according to fill factor. The PR functioned as both protection and mechanical support layer during EC etching. It was removed after the completion of the transfer-printing for material characterization and fabrication of subsequent devices (Figure 7(e)).

2. Flexible Optoelectronics

2.1. Flexible Optoelectronics using 1-D semiconductors

The first category to consider for flexible optoelectronics is that of 1D materials which is generally defined as structures in the form of NWs, nanorods, nanobelts, and nanoribbons as discussed in section 1 and are named as such due to the confinement of charge carriers to only one spatial dimension due to the nature of the structure. These materials extend relatively long in one dimension but are confined in the other two. For the purpose of this review, we will also treat quantum dots and core-shell structures, which are sometimes classified as zero-dimensional (0D), as 1D materials. These structures can be synthesized from many common materials such as III-Vs, oxides, metals, and also graphene. Here we examine several applications of 1D materials in

optoelectronics, namely photodetectors, solar cells, LEDs, and lasers, which can be seen in Figure 8 along with the materials considered for each type of device.

2.1.1D Photodetectors and photovoltaics

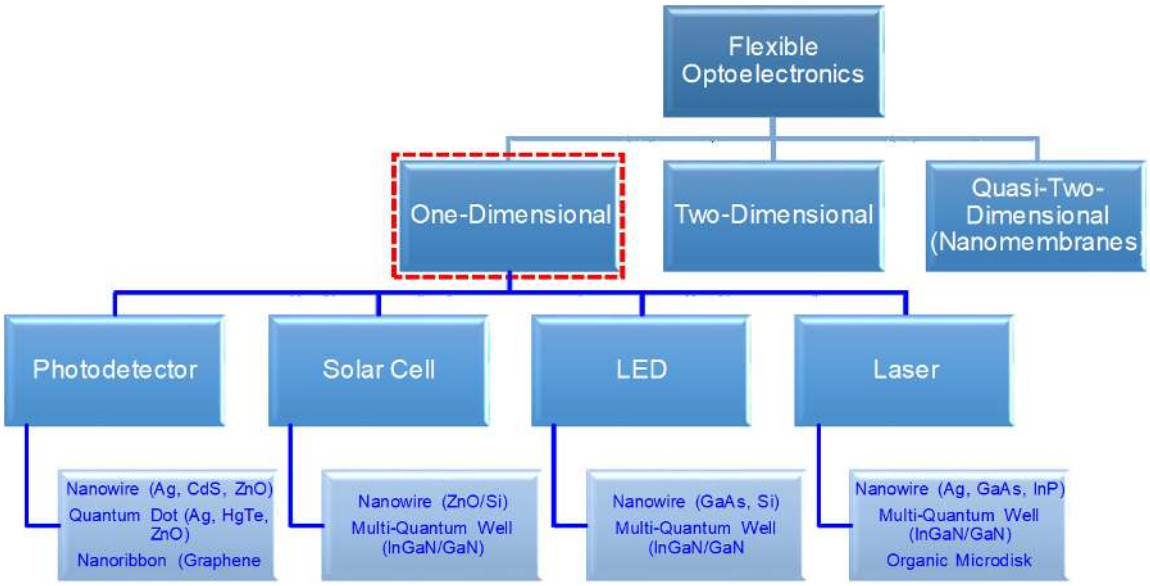

Figure 8. Three main categories of flexible optoelectronics, along with several common device types and materials used in the fabrication of each device.

The first structure to consider for 1D photodetectors are NWs, materials that have diameters on the nanometer scale but can have lengths of more than 1 μm. Their photodetection characteristics are largely decided by their bandgap but also affected by the configuration of charge transport mechanism, because of the surface potential associated with their nanoscale dimension.

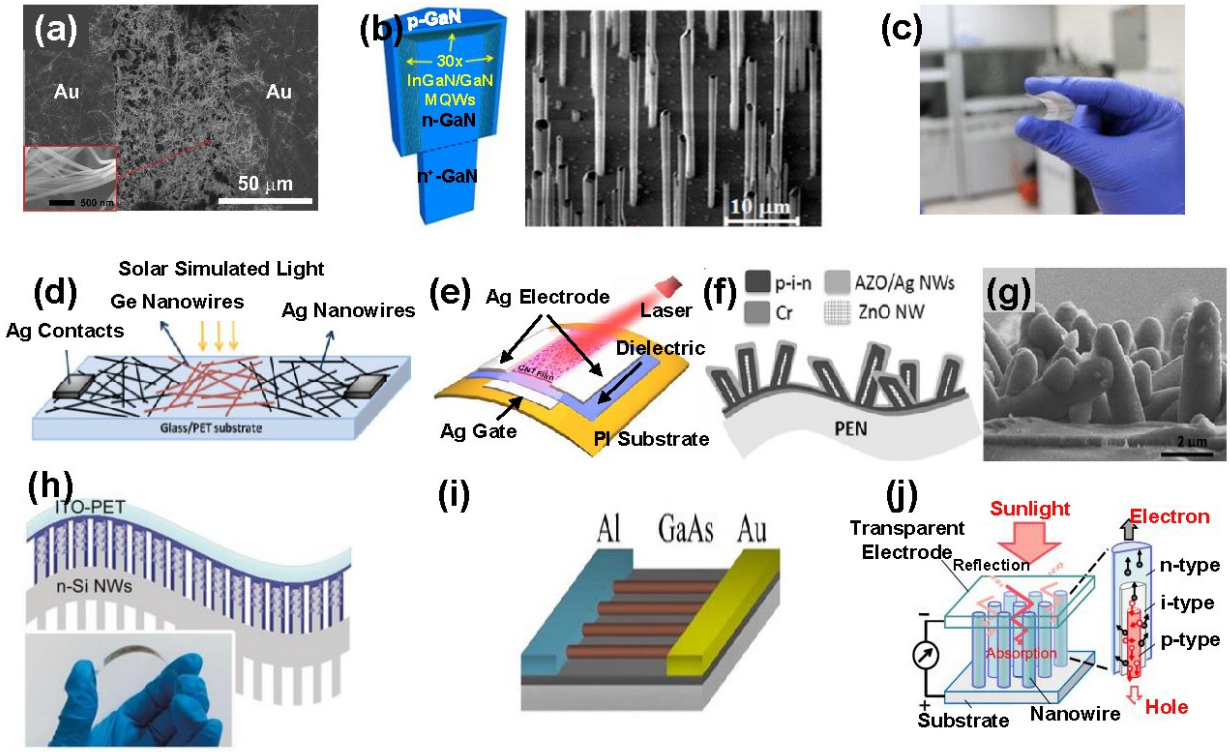

Figure 9. (a) SEM image of ZnO NWs (center) with Au contacts [74]. (b) Illustration of core-shell InGaN/GaN NW structure and SEM image of InGaN/GaN NWs [75]. (c) Image of flexible Si NW on PET [76]. (d) Illustration of flexible photodetector with Ge NWs as the active material along with Ag NWs and SWNTs as charge transport layers [77]. (e) Illustration of CNT photodetector on flexible PI substrate [78]. (f) Device structure of hybrid ZnO/a-Si NW flexible photodetector on PEN substrate and (g) SEM image of the structure [79]. (h) Si NW device structure on flexible ITO-PET substrate along with image of the device under bending [80]. (i) Device structure of GaAs NW photodetector. (j) Schematic of InP NW photodetector [81].

As shown in Figure 9(a-c), the ZnO and GaN NW based flexible photodetectors show strong solar-blind light absorption characteristics [74-76], while Ge NW based ones show good visible blind property [77]. The use of CNT offers fast photodetection due to their high mobility value [78]. The advanced NW design routes such as a multicore layer hybrid structure (GaN/InGaN NWs) or (CdS NWs/WSe_2) were proposed in order to create or boost the surface states which leads to a further improvement of photogeneration in the active region. Similar to photodetectors, 1D materials are also used in the fabrication of solar cells. However, the bandgap of active region needs to cover visible wavelengths, thus the most popular based active material is Si. As shown in Figure 9(f-g),

it is common to form a hybrid structure based on Si such as ZnO NW/a-Si:H hybrid structure. This device was built on a polyethylene naphthalate (PEN) substrate [79] and the hybrid structure of the device allows for the absorbance range to be extended similarly to a multi-junction solar cell, with absorption in the UV from the ZnO and in the visible range from the Si. Similarly, poly(3,4-ethylenedioxythiophene)/poly-(styrene sulfonate) (PEDOT:PSS), which absorbs light in the near-IR spectrum, is deposited to coat the Si NWs to enhance the absorption performance [80]. Beside Si NWs, III-V compound such GaAs or InP are other popular materials that absorb broader spectrum effectively. Their biggest advantage is the ability of forming a multilayer structure such as $In_xGa_{1-x}P$-$Al_yGa_{1-y}As$-$In_zGa_{1-z}As$ NWs which can form a multi-junction flexible solar cell, with a theoretical efficiency of over 50% [81].

2.1.2 Light Emitting Diodes

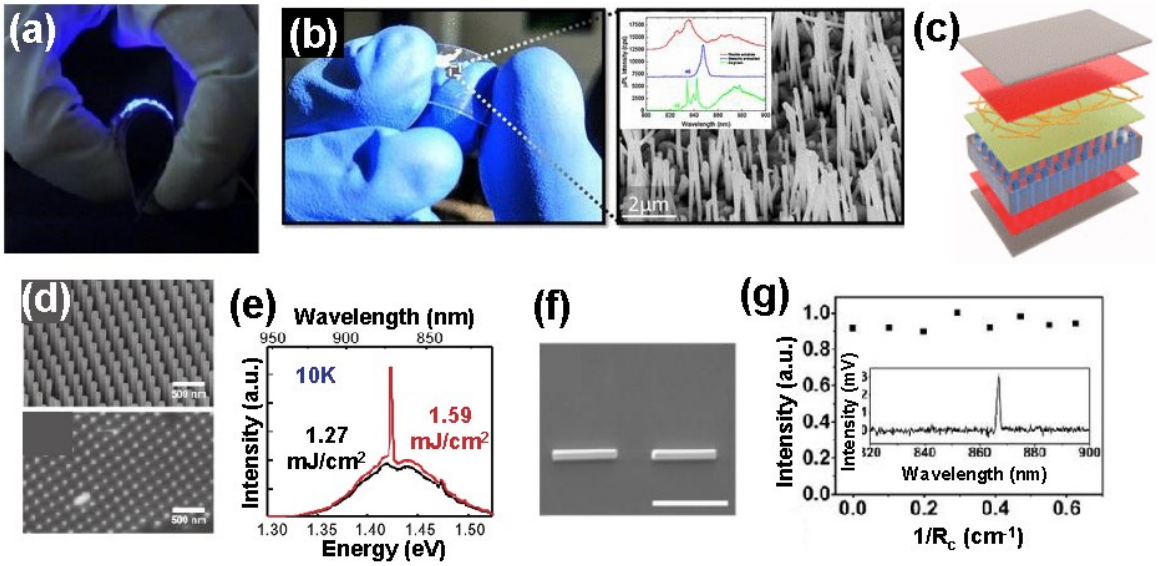

Figure 10. (a) Photographs of InGaN/GaN MQW LED in operation under bending [83]. (b) Image of flexible GaAs NW LED along with SEM image of NWs and emission spectrum of the device [87]. (c) Structure of ZnO/Si NW LED [88]. (d) SEM image of GaAs NWs with InGaAs/GaAs QDs and (e) the output spectrum of the device [89]. (f) SEM image of InP NWs and (g) output spectrum along with the output light intensity vs. the bending radius [90].

Toward the demonstration of flexible light emitting devices, the most common materials used are III-nitride semiconductors NWs (InGaN/GaN), and also III-V NWs (GaAs/InGaAs). These NW-based light emitting devices cover the spectrum ranging from the visible to near-IR wavelength. In the same manner as reported for InGaN/GaN NW photodetectors [82], flexible LEDs containing InGaN/GaN NW multi-quantum wells are fabricated by techniques such as MOCVD on a rigid donor substrate as discussed in section 1 [83-85]. These NWs contain many alternating layers of InGaN and GaN in a so-called core-shell pattern to form a multi-quantum well. One such device produces a blue LED, with a sharp emission peak at 415 nm and a broader peak from 400-500 nm with high external quantum efficiencies (EQE) of over 80% [83, 86]. A similar concept can be utilized to create stacked LED structures using InGaN/GaN NWs as the active media, each layer producing a different wavelength to produce multiple color outputs (Figure 10(a) [83]) To produce a red to a near-IR light emission, GaAs/InGaAs NWs can be used as the active material, as is with the device shown in Figure 10(b). The fabrication process for this type of flexible LED is slightly different than for InGaN/GaN NWs, with the detachment of the NWs from the substrate via plasma etching followed by the transfer of the free-standing NWs to a flexible plastic substrate [87]. For this device, high efficiency light emission is possible with peaks in the region of 830-850 nm, with emission from the GaAs growth clusters resulting in a broad peak, or from the NWs resulting in a sharp peak [87]. For UV light emission, ZnO NWs are also used for flexible LED fabrication. By embedding ZnO NWs in various polymer substrates, it is possible to produce flexible white LEDs resulting from emission from the NWs (~450nm) as depicted in Figure 10(c) [88]. Beside light emission, flexible 1D lasers are also possible with the same structure for the active material by implementing core-shell NWs. Figure 10(d) shows an SEM image of GaAs NWs with a $In_{0.2}Ga_{0.8}As$ multi-quantum well and GaAs/$Ga_{0.1}Ga_{0.9}As$/GaAs

core-shell-cap layers grown by MOVPE. The NWs were embedded in a PDMS substrate and lasing was observed with a sharp stimulated emission peak at 870 nm and a broader background peak resulting from spontaneous emission from the NWs [89], as seen in Figure 10(e). InP lasers are also possible on flexible substrates, and have been demonstrated with waveguide coupling to enhance output. Figure 10(f) shows an SEM image of InP NWs that can be coupled with a waveguide on a flexible glass substrate resulting in emission peaks at 861 nm and 882 nm with minimal variation in power output during bending up to 1.6 cm of radius, at which point the glass substrate fractures [90].

2.2. Flexible Optoelectronics using 2-D semiconductors

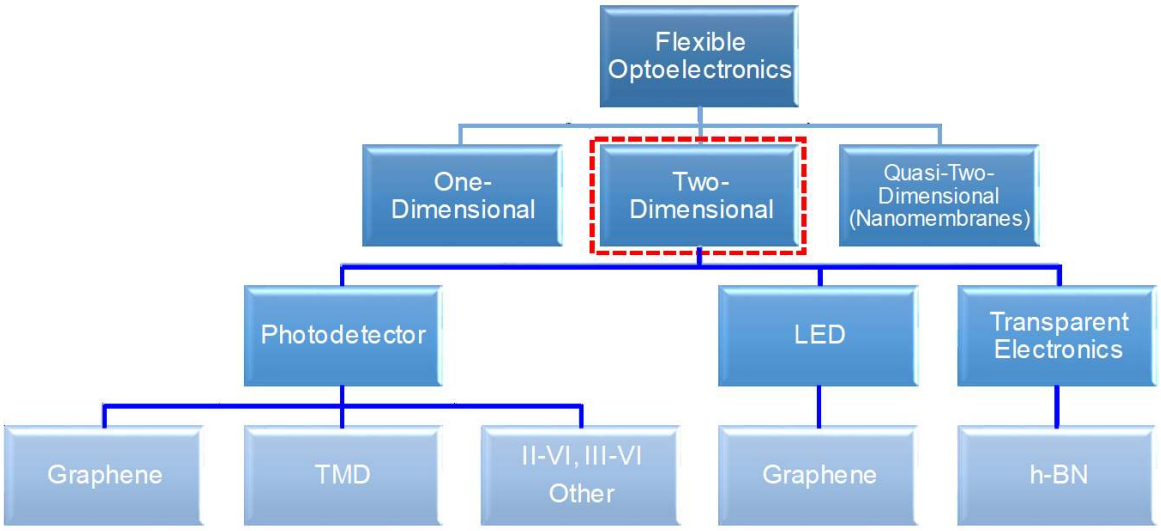

Figure 11. Three main categories of flexible optoelectronics, along with several common device types and materials used in the fabrication of each device.

The category of 2D material based flexible optoelectronics contains planar forms of semiconductors such as nanosheets and nanoplates [91] where the charge carriers are confined to only two spatial dimensions. As discussed in section 1, 2D materials commonly include graphene, TMDs such as MoS_2 or WSe_2, II-VI group such as CdSe, hexagonal boron nitride (h-BN), and more, as shown in Figure 11 and 12. Owing to their atomic thinness, 2D materials possess great

mechanical stability and durability which are ideal material choice in the fabrication of flexible optoelectronic devices such as photodetectors, LEDs, and transparent electronics.

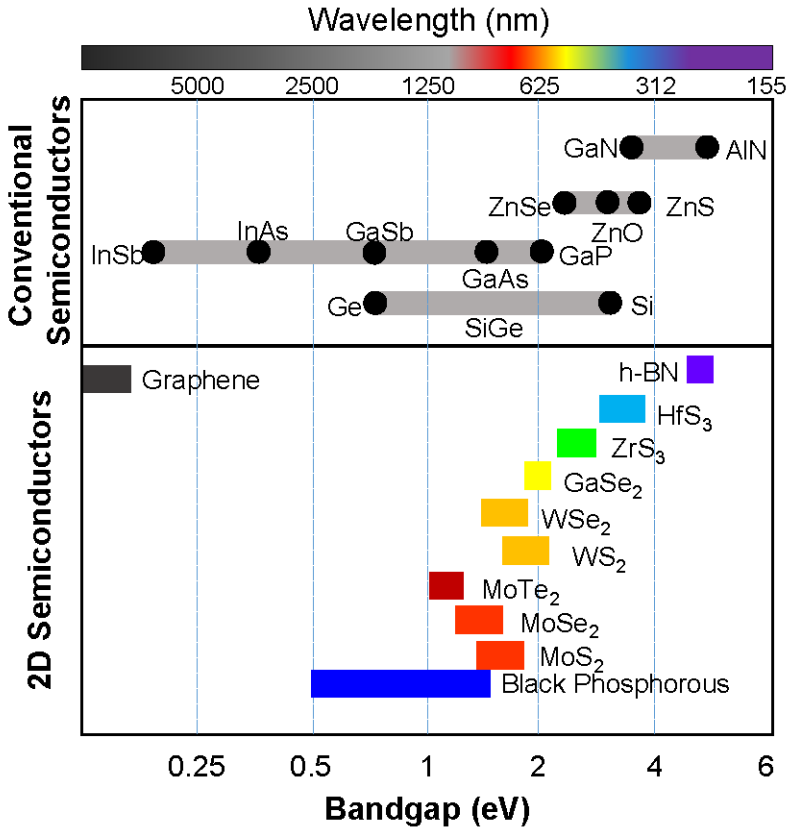

Figure 12. Bandgap and absorption wavelengths for many semiconductors, including 2D and TMD materials.

2.2.1 Photodetectors

The most common application of 2D materials in flexible optoelectronics is towards photodetectors. Materials such as graphene, TMDs, and others are used for this purpose. Figure 13 shows common graphene photodetectors on flexible substrates, with Figure 13(a), showing a crumpled photodetector on an elastomer substrate. The device exhibits a responsivity of only 0.019 mA/W but has excellent mechanical performance, with the photocurrent unchanged after more than 1000 bending cycles and a capability of handling strains of up to 200% [92]. The responsivity is able to be improved to 0.044 mA/W with the addition of the Au plasmonic structure [92]. It is

also possible to dope graphene in order to create a PN junction, which can be operated as a photodetector, as shown in Figure 13(b) [93]. In this case, the graphene that is CVD-grown and transferred in air is considered as the p-type material. To achieve n-type doping, 2-(2-methoxyphenyl)-1,3-dimethyl-2,3-dihydro-1H-benzoimidazole (o-MeO-DMBI) is chosen as the n-type dopant and can be exposed to the graphene via vapor deposition or inkjet printing methods.

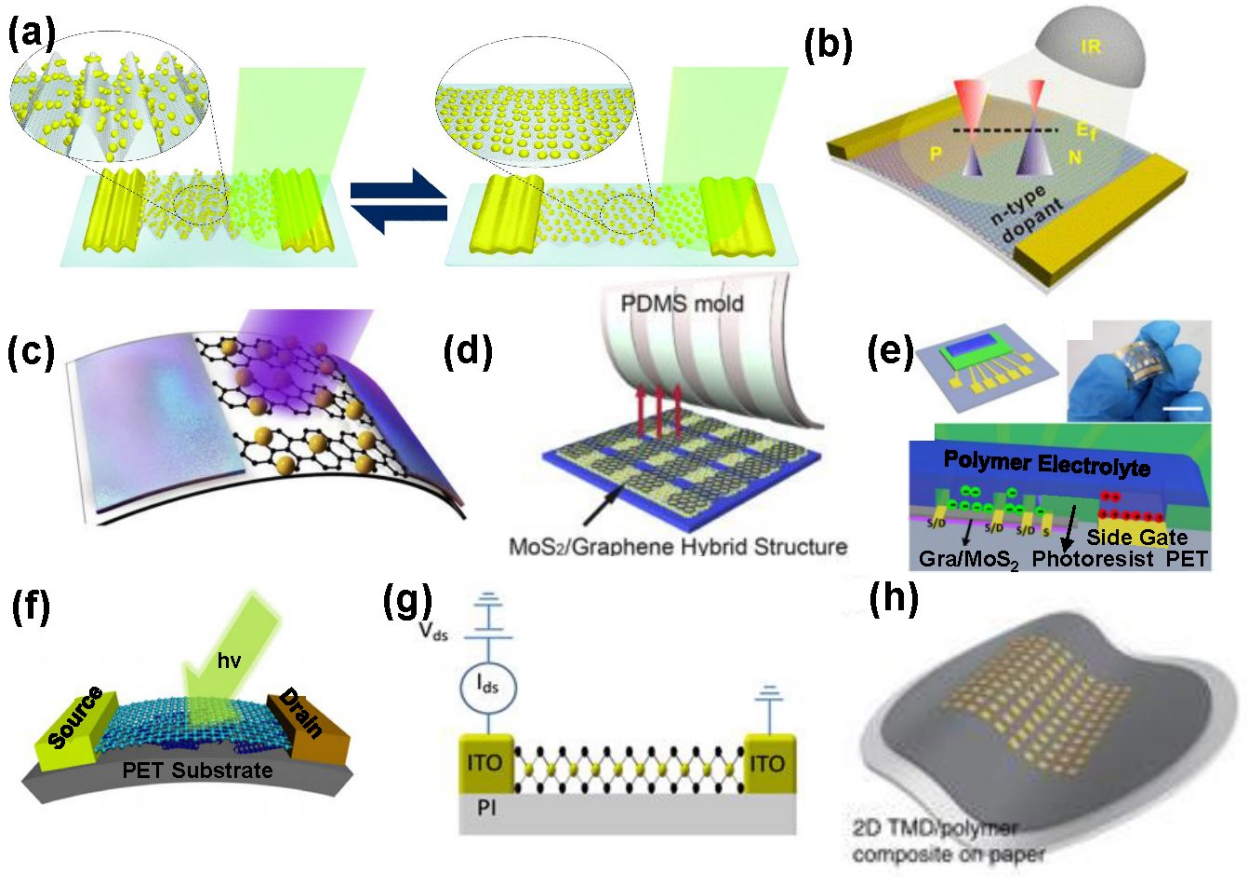

Figure 13. (a) Crumpled-graphene photodetector device structure while relaxed and under strain [92]. (b) Device structure of doped-graphene PN junction photodetector [93]. (c) Illustration of hybrid graphene-MoS_2 QD photodetector [94]. (d) Hybrid graphene-MoS_2 nanosheet hybrid structure on PDMS [95]. (e) Hybrid graphene-MoS_2 photodetector on PET [96]. (f) Graphene-SWNT photodetector device structure [98]. (g) Typical device structure of TMD photodetector, in this case WSe_2 on PI substrate [99]. (h) $MoSe_2$ nanosheets exfoliated with amine-terminated polymers to form composite structure [101].

Graphene is also commonly used in conjunction with other materials to form a hybrid photodetector. It is possible to add other nanomaterials such as nanoparticles or other 2D materials

to graphene to enhance the optical properties and device performance. Figure 13(c) shows a hybrid graphene/MoS_2 quantum dot photodetector fabricated by the unzipping of carbon nanotubes and the deposition of MoS_2 quantum dots by a solution process showing six orders of magnitude higher than a pure graphene photodetector [94]. As another example, MoS_2 nanosheets have also been combined with graphene to create hybrid photodetectors as shown in Figure 13(d)-(e), exhibiting superior responsivities at low voltage bias [95-96]. In addition, a reduced graphene oxide (rGO) was used to realize UV photodetector with an excellent mechanical performance on a flexible substrate [97]. Other than employing rGO, TiO_2 particles or SWNTs have been employed to modify graphene based photodetectors as shown in Figure 13(f). These devices demonstrate a high responsivity with a robust performance under bending condition [98].

TMD materials are also used to fabricate flexible photodetectors. Figure 13(g) shows the device structure of a monolayer WSe_2 photodetector on a polyimide (PI) substrate. It is possible to only have a monolayer of the material present in the device, but in the case of this device the thickness of the WSe_2 nanosheet is 48 nm. This photodetector is sensitive over a broad range from 370-1064 nm with a peak responsivity of 0.92 A/W at 635 nm, which only decreases by 5% at a bending radius of 5 mm [99]. Similar TMD photodetectors with MoS_2 nanosheets on PET are also possible, with thicknesses of 1-5 nm [100] which is much thinner than for the previous device. This flexible photodetector indicates a responsivity of 0.02 A/W, similar to other MoS_2 photodetectors [100]. Figure 13(h) shows a flexible photodetector with TMDs such as MoS_2, $MoSe_2$, WS_2, and WSe_2 hybridized with amine-terminated polymers polystyrene (PS), poly(methyl methacrylate) (PMMA), poly(butadiene) (PBd), poly(ethylene) (PE), poly(ethylene oxide) (PEO), and poly(styrene-*b*-isoprene) (Ps-*b*-PI). The resulting devices with composite active

materials are highly photoconductive with a responsivity of 16 A/W for $MoSe_2$ nanosheets coated with PS and are stable at bending radii as low as 200 μm under near-IR and visible light [101].

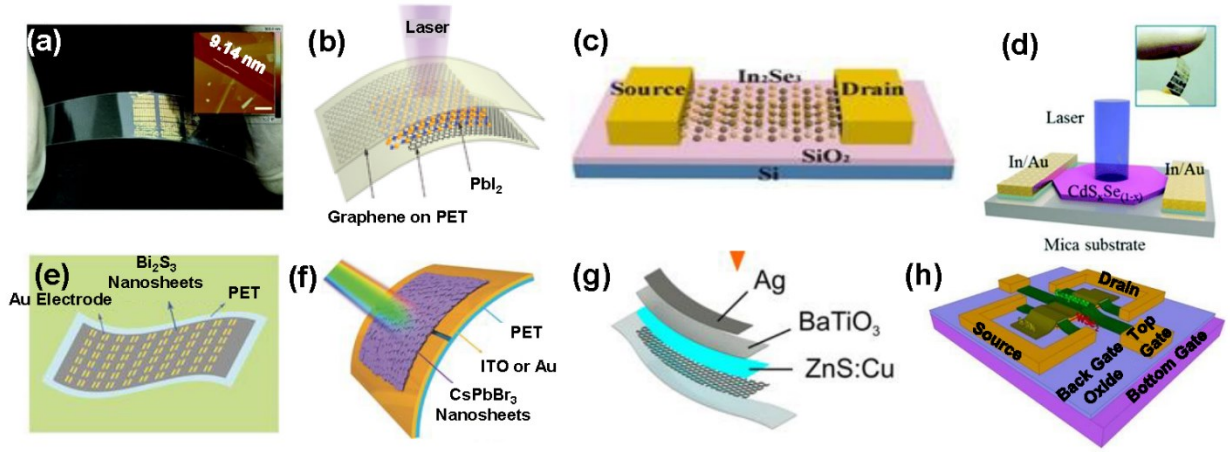

Figure 14. (a) Image of PbI_2 on PET substrate, along with AFM image of PbI_2 nanosheets [102]. (b) Illustration of PbI_2 on graphene photodetector structure [103]. (c) In_2Se_3 photodetector structure [104]. (d) $CdS_xSe_{(1-x)}$ structure [105]. (e) Bi_2Se_3 photodetector device structure [106]. (f) Illustration of $CsPbBr_3$ on PET/ITO substrate [107]. (g) Device structure of flexible LED with ZnS:Cu nanosheet as the active layer [108]. (h) Illustration of device structure of transparent h-BN TFT with graphene as metal electrode, h-BN as gate dielectric and WSe2 as the semiconducting channel material [109].

Other nanosheet materials are often used to produce flexible photodetectors with much higher responsivities than for TMD materials. Figure 14 shows common materials used for flexible 2D photodetectors, with responsivities of 131.7 A/W for PbI_2 over the visible region [102-103] (Figure 14(a)-(b)), 363 A/W for In_2Se_3 over the UV-visible region [104] (Figure 27(c)), 703 A/W for $CdS_xSe_{(1-x)}$ over the visible region [105] (Figure 14(d)), 4.4 A/W for Bi_2Se_3 over the visible-near-IR region [106] (Figure 14(e)), and 0.25 A/W for $CsPbBr_3$ suitable for green photodetection [107] (Figure 14(f)). For these devices, any performance changes are negligible under bending after 10,000 bending cycles [107] with the exception of $CdS_xSe_{(1-x)}$ which suffered some decrease in light and dark current after 50 cycles [105], although this device was fabricated on a mica substrate which is more brittle and prone to failure than a polymer substrate such as PET.

2.2.2 Other Flexible optoelectronic applications based on 2D semiconductors

Few applications exist for flexible 2D optoelectronics outside of photodetection, with the exception of LEDs and transparent thin film transistors (TFTs). Figure 14(g)-(h) shows some examples of these applications with a flexible Cu-doped ZnS (ZnS:Cu) nanosheets LED (Figure 14(g) [108]) and a transparent flexible h-BN-WSe_2 TFT (Figure 14(h) [109]). The LED emitted light centered around 500 nm and suffered no significant degradation under bending, torsion, and cyclic loading [108]. Therefore, although the research in flexible 2D light source is in the premature stage, it shows a great promise toward a future flexible light source. Also, considering a bandgap tunability of some of 2D materials such as phosphorene, it is probably possible to demonstrate flexible tunable light source based on 2D materials.

2.3. Quasi-Two Dimensional Materials

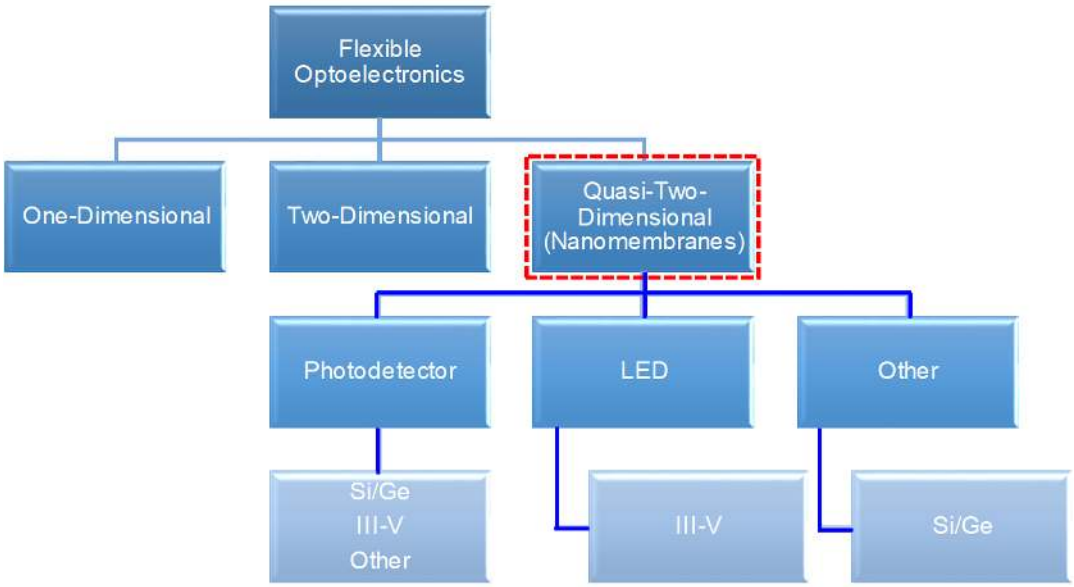

Figure 15. Three main categories of flexible optoelectronics, along with several common device types and materials used in the fabrication of each device.

A third category of flexible optoelectronic devices uses quasi-two-dimensional (Q2D) materials as the active material. This category consists of structures such as NMs, similar to the

nanosheets of 2D materials but do not consist of only a few layers and are in the range of tens to hundreds of nanometers in thickness. Similar to 1D and 2D materials, it is common to fabricate flexible photodetectors, photovoltaics, LEDs, and other devices from conventional semiconductor materials such as Si, Ge, and III-Vs. Figure 15 shows the categories of devices and materials used for each device. Under normal conditions, a bulk single-crystal Si or GaAs wafer is very brittle and cannot handle much strain before fracture. However, these materials can be fabricated in such a method as to yield NMs with extremely small thicknesses and can be more than 15 orders of magnitude more flexible than the bulk substrate [110]. Once a NM of sufficient thickness is achieved, it can be integrated with flexible substrates to produce flexible electronic and optoelectronic devices.

2.3.1 Photodetectors

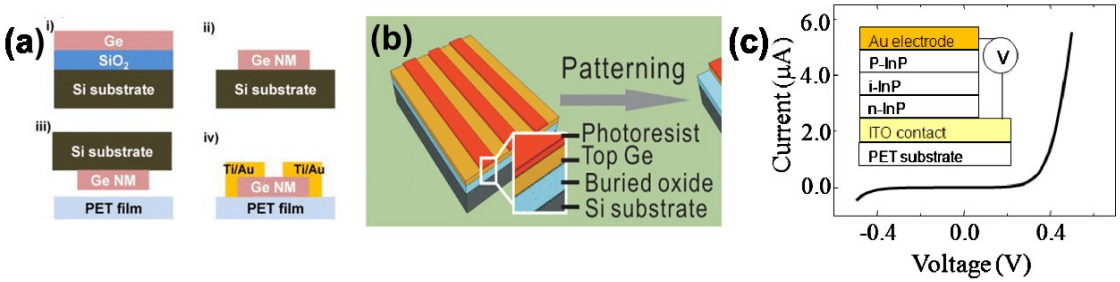

Figure 16. (a) Device structure of Ge NM photodetector on PET [65]. (b) Device structure of Ge photodetector [111]. (c) Device structure and current-voltage characteristics of InP NM photodetector [112].

As with 1D and 2D materials, photodetector is the typical device to be fabricated from Q2D materials. Most Q2D flexible photodetectors are fabricated using single-crystal NMs from materials such as Si, Ge, or III-V semiconductors. Their absorption spectrum is primarily decided by their bandgaps, thus, as shown in Figure 16(a-b), Si NM and Ge NM offer superior near infrared detection with the responsivity greater than a few A/W [65, 111]. The advantage of these Q2D flexible photodetectors is the stable photodetection under the bending condition due to their

excellent mechanical properties compared to other III-V based NMs, namely less fragility, and relatively high absorption coefficient. III-V materials, specifically InP, GaN, GaAs, InGaAs, and AlGaAs can be processed and fabricated into NMs and can be achieved decent flexibility. As III-V materials can form various alloys, this material set offers a great freedom to design their absorption peak or bandwidth by controlling their bandgap and thickness. Figure 16(c) shows an example of a PIN photodetector on PET fabricated from InP NMs, along with the current-voltage characteristics of the device. The responsivity values of this device exceeds 0.1 A/W at near IR. Also, there is little loss in responsivity after 1000 bending cycles and similar current-voltage characteristics for both linear and bent devices, presenting good stability of the devices [112]. GaN compound NMs has a capable of a solar-blind photodetection due to their wide bandgap properties. GaN/AlGaN compound semiconductors can selectively absorb UV light and transparent to visible range. Although these wide bandgap NMs are not as flexible as other Si, Ge, or III-V materials due to their high poison ratio, flexible UV photodetector can open up the new avenue to the brain signal detection in the biomedical area due to the solar-blind photodetection with a great visible light rejection ratio.

Here it is worth noting a very promising application of Q2D NM based photodetectors in the field of biomimicry. It is possible to exploit the mechanical properties of sufficiently thin semiconductor nanomembranes to fabricate an array of photodetectors, as would be used for various imaging purposes, and conform them to a flexible polymer substrate mimicking the surface of the human eye, as does a contact lens. Figure 17 displays several such devices involving various materials and optimized device structures. By combining with a separated fluid reservoir, advanced version of electronic eyes that are capable of changing the magnification level of the detected image, as shown in Figure 17(i) [113].

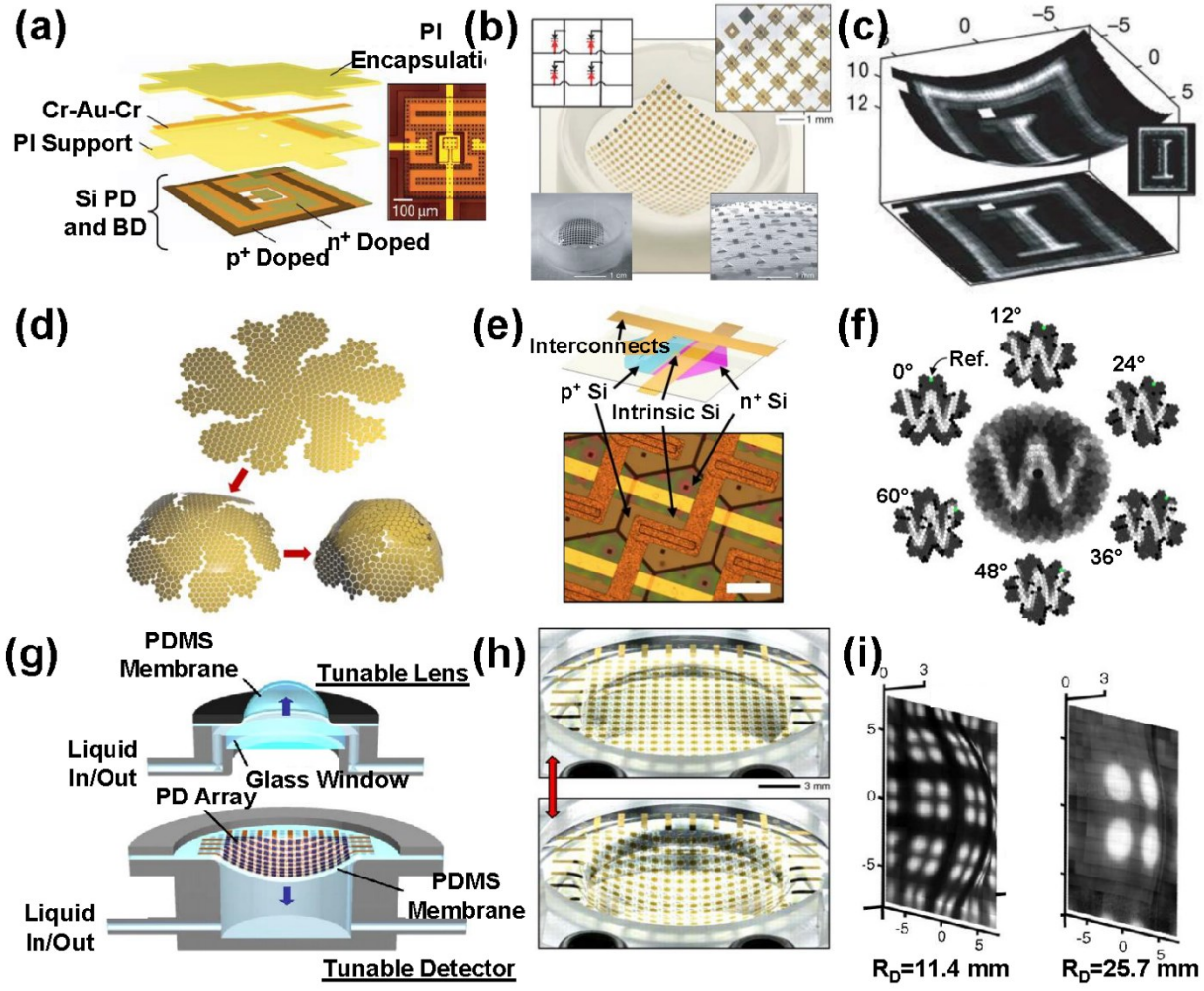

Figure 17. (a) Device structure of Si NM based flexible electronic eye. (b) Optical image of flexible photodetector array for use as an electronic eye, along with detailed optical and SEM images of the array. (c) Original image (bottom and side) and image detected by electronic eye (top) [114]. (d) Device layout of flexible Si NM photodetector array the design of which has been modified into a half truncated icosahedron and folded into a hemisphere. (e) Detailed optical image and illustration of the device layout of the photodetector array. (f) Image of the letter 'W' captured by the hemispherical electronic eye [62]. (g) Illustration of flexible Si NM camera with a polymer lens. (h) Higher magnification view of the photodetector array under the flat condition and under bending. (i) Low-magnification (left) and high magnification (right) images from the electronic eye obtained by adjusting the radius of curvature via the fluid pressure [113].

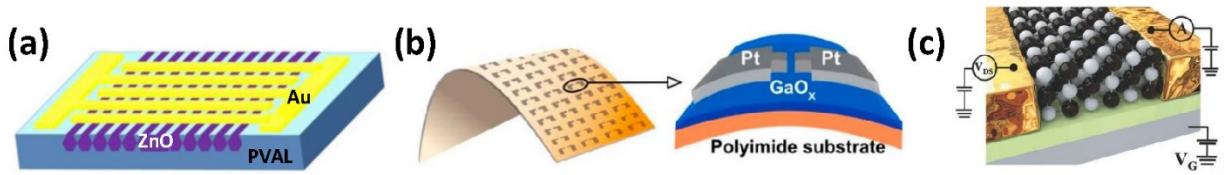

Figure 18. (a) Device structure of ZnO photodetector [115]. (b) Device structure of amorphous GaOx thin film photodetector [117]. (c) Illustration of SnTe NM photodetector [118].

Moving away from the popular Si, Ge, and III-V materials, other compound materials such as ZnO, GaO_x and SnTe can be used as active materials for flexible Q2D photodetectors. Figure 18(a) shows a flexible ZnO microwire photodetector on a polyvinyl alcohol (PVAL) substrate. Normally, a wire-type structure would be categorized under 1D materials, but the dimensions of the ZnO structures employed in this device are on the micron scale, with the diameter ranging from 40-50 μm and the length from 3-5 mm, justifying the name microwire and its treatment as a Q2D material. The single-crystal microwires are grown by CVD and transferred to a PAVL substrate, where it operates as a flexible UV photodetector with a sharp absorption cutoff at wavelengths above 380 nm [115]. Figure 18(b) shows a flexible GaO_x thin film photodetector on PI substrate. Although there has been an increasing amount of attention on single-crystal β-Ga_2O_3 for flexible applications [116], it is still possible to use amorphous GaO_x thin films for various devices. This device demonstrates a detection capability over UV wavelengths in the range of 200-300 nm, with a peak responsivity of 45.11 A/W a 235 nm, and can withstand bending with a radius as low as 14 mm with stable performance [117]. SnTe is an additional material from which Q2D photodetectors can be fabricated, integrating nanoflakes instead of NMs. Figure 18(c) shows the structure of a flexible SnTe on PET photodetector with the nanoflake thickness ranging from 120-2200 nm. This device offers photodetection capabilities over a wide range from 254-4650 nm, making it suitable for a UV-near-IR photodetector [116]. However, the device's peak responsivity of 71.11 A/W occurs at 254 nm and decreases to 4.17 A/W at 4650 nm wavelength [118]. The high responsivity

is due to the p-type doping of SnTe, which in many topological crystalline insulators can greatly increase the responsivity by suppressing the rapid recombination of holes generated from light absorption [118].

2.3.2 Q2D based Flexible Photovoltaics and Light Emitting Devices

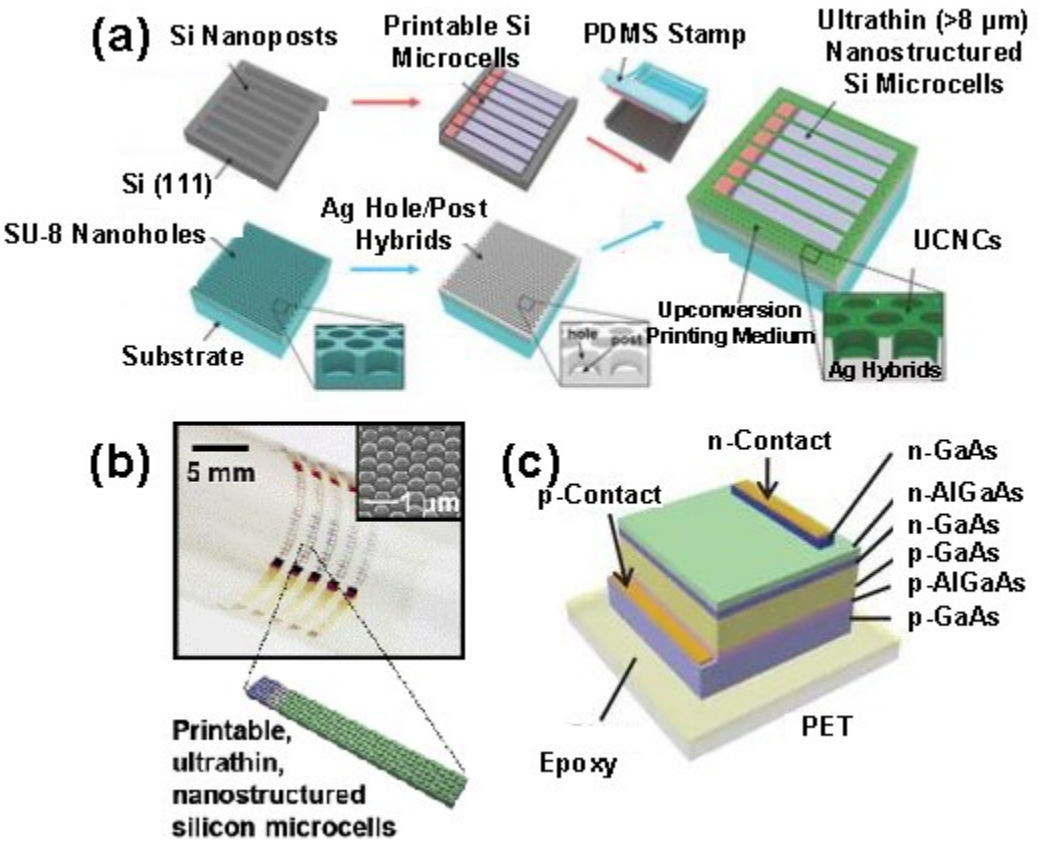

Figure 19. (a) Fabrication procedure for patterned Si nanostructure solar cells. (b) Image of printable nanostructured Si wrapped on glass rod [119]. (c) Device structure of flexible GaAs NM solar cell [120].

It is common to use Si and III-V NMs in the fabrication of flexible photovoltaic devices as well. Figure 19 shows several flexible solar cells with Si and GaAs as the active materials. Similar to the rigid version of photovoltaics, light absorption was enhanced with the addition of lanthanide-doped $NaYF_4$ upconversion nanocrystals ($NaYF4:Yb^{3+},Er^{3+}$) yielding a solar-to-electric conversion efficiency of 12%, which is an increase of 130% over bare Si microcells on a SU-8

substrate, 41% over nanostructured Si solar cells on a bare Ag substrate, and 13% over nanostructured Si solar cells on a nanostructured Ag substrate [119] (Figure 19(a-b)). Therefore, further enhancement is expected by optimizing the dimensions and distributions of features on nanostructured Si membranes. For example, the thicknesses of these active layers varying between 40 nm to 2 μm result in an EQE of 14.5% to 20.5% with the addition of antireflection coatings [120] (Figure 19(c)).

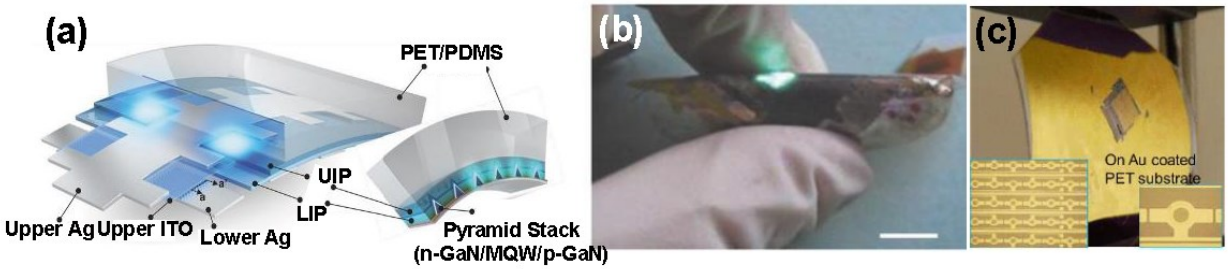

Figure 20. (a) Illustration of flexible GaN LED. (b) Image of device operation under bending [121]. (c) Optical images of InP NM LED device [122].

The material selection of Q2D material-based flexible LEDs varies by their light emission wavelength. Typically, III-V materials such as GaAs or InP NMs emit near infrared (IR) to orange light and III-nitride materials such as GaN/InGaN emit green or UV light. It should be noted that these NMs must have a pre-grown high quality multi-quantum wells in the NMs in order to generate photons. Therefore, maintaining the LED structure without being cracked or deformed during a transfer printing process is a key step to realize flexible light emitting devices. Figure 20(a-b) shows a flexible InGaN/GaN NM LED on a PET/PDMS substrate. This device uses InGaN/GaN pyramid structures as a multi-quantum well for light emission and exhibited maximum light emission intensities at 483 nm and 514 nm and showed a stable emission performance after bending [121]. Figure 20(c) shows a flexible InP NM LED on a PET substrate. For this device, InP NMs are transferred onto a PET substrate and combined with InGaAsP NMs

to form a multi-quantum well structure. This LED is suitable for near-IR emission, with an electroluminescence peak at 1527 nm [122].

3. Conclusion and Future Perspective

In this paper, we primarily reviewed the recent advances in the development of freestanding inorganic crystalline semiconductors and their manipulation technology. We firstly covered the details of the growth, processing of freestanding inorganic crystalline semiconductors in various dimensions: (1D semiconductors such as Si-, GaAs-, ZnO-, and GaN-NWs, 2D semiconductors such as graphene, MoS_2, and quasi-2D semiconductors such as perovskite, PbI2 NM, In2Se3 NMs ZnS NMs, Ge NMs, III-V NMs, III-nitride NMs and ZnO NMs), and their material property under strain condition. Finally, fabrication processes and opto-electrical properties of flexible optoelectronics such as flexible photosensors, lighting devices, and photovoltaics was introduced.

Given that research in flexible optoelectronics is in its early stage, two future research directions could be suggested to drive the flexible optoelectronics to the next level. For one, high-performance low-dimensional semiconductors could be developed. In addition, the device structure could be engineered to build advanced flexible optoelectronics. A major challenge with the materials and device structures is the limited physical form factors of freestanding semiconductors. In other words, light-matter interaction inside all the freestanding semiconductors introduced in this review is weak because they have sub-micron thicknesses regardless of their material and mechanical properties. In fact, flexible photovoltaics or photosensors suffer from poor quantum efficiency primarily due to poor light absorption in the active region. This limitation has been overcome through several recently proposed approaches. One is to re-design the structure of the device by manipulation during fabrication such as a flip-transfer. A flip-transfer allows us to

access both the top and bottom surfaces of the active material and enables to form an anti-reflective layer that can boost light absorption. This approach was recently utilized by Seo et al. by forming a reflector on the bottom and an anti-reflective coating on the top of a photosensor, doubling its photosensitivity [70]. Similarly, various optically functional layers can be formed on both sides of freestanding semiconductors to simply enhance their optical properties. Implementing a photonic concept with flexible optoelectronics is another route to boosting the opto-electrical performance of these devices [123]. Photonic crystals on the surface of freestanding semiconductors can tune their absorption coefficients, improving their effective light absorption depth. In this way, thin freestanding semiconductors can absorb more photons up to the levels in their bulk counterparts. Conversely, some groups are trying to utilize this limited light absorption which can be beneficial for designing new applications for flexible optoelectronics. Because freestanding semiconductors can be precisely placed using a micro-transfer printing method, stacked freestanding semiconductors with various optical bandgaps can be used to demonstrate multicolor photosensors or multijunction solar cells which are difficult to realize with traditional optoelectronic materials. Rigid versions of these photosensors and photovoltaics were recently realized by Menon et al. and Chang et al. [124-125] which showed that this concept can be applied to flexible optoelectronics, taking advantage of transferable/stackable freestanding semiconductors.

In the other research direction is to develop the process integration technology for advanced optoelectronic systems. The next-generation high-performance computer is expected to have more optical parts compared to existing computer solutions. Together with flexible electronic devices, flexible optoelectronic devices will play major roles in future IoT devices that will be able to monitor various environmental data, receive/transmit information, and display 3D or high definition (HD) pictures and videos. To realize these applications, seamless side-by-side or vertical

integration will be an important process technology. Although several research groups have been pioneering a variety of integration approaches for combining various types of partially- or fully-fabricated devices, more efforts should be made toward the development of an advanced integration process. Integration, not only between electronic and optoelectronic devices, but also within photonic components, will lead to a substantial technological leap.

Acknowledgement

This work was supported by the National Science Foundation (Grant number: ECCS-1809077) and partially by Young Investigator Award of Korean American Scientists and Engineers Association and the Start-up Grant (PI: Prof. Munho, Kim) of Nanyang Technological University (NTU), Singapore.

References

1. Brennan KF. The physics of semiconductors: with applications to optoelectronic devices. Cambridge university press; 1999.
2. Bhattacharya P, Pang LY. Semiconductor optoelectronic devices. Vol. 613. prentice hall Upper Saddle River, NJ; 1997.
3. Wong WS, Salleo A. Flexible electronics: materials and applications. Vol. 11. Springer Science & Business Media; 2009.
4. Hamers RJ. Flexible electronic futures. Nature. 2001;412(6846):489.
5. Kim D-H, Lu N, Ma R, et al. Epidermal electronics. science. 2011;333(6044):838-843.
6. Ko HC, Stoykovich MP, Song J, et al. A hemispherical electronic eye camera based on compressible silicon optoelectronics. Nature. 2008;454(7205):748.
7. Dong L, Agarwal AK, Beebe DJ, et al. Adaptive liquid microlenses activated by stimuli-responsive hydrogels. Nature. 2006;442(7102):551.
8. Crawford GP. Flexible flat panel display technology. Vol. 3. Wiley Online Library; 2005.
9. Labroo P, Cui Y. Flexible graphene bio-nanosensor for lactate. Biosensors and Bioelectronics. 2013;41:852-856.
10. Hwang SW, Huang X, Seo J.-H., et al. Materials for bioresorbable radio frequency electronics. Advanced Materials. 2013;25(26):3526-3531.
11. Gudiksen MS, Wang J, Lieber CM. Synthetic control of the diameter and length of single crystal semiconductor nanowires. The Journal of Physical Chemistry B. 2001;105(19):4062-4064.
12. Law M, Goldberger J, Yang P. Semiconductor nanowires and nanotubes. Annu Rev Mater Res. 2004;34:83-122.

13. Shi W, Peng H, Wang N, et al. Free-standing single crystal silicon nanoribbons. Journal of the American Chemical Society. 2001;123(44):11095-11096.
14. Kong XY, Wang ZL. Spontaneous polarization-induced nanohelixes, nanosprings, and nanorings of piezoelectric nanobelts. Nano letters. 2003;3(12):1625-1631.
15. Sun Y, Sun Z, Gao S, et al. Fabrication of flexible and freestanding zinc chalcogenide single layers. Nature communications. 2012;3:1057.
16. Wang F, Seo J.-H., Luo G, et al. Nanometre-thick single-crystalline nanosheets grown at the water–air interface. Nature communications. 2016;7:10444.
17. Tao L, Cinquanta E, Chiappe D, et al. Silicene field-effect transistors operating at room temperature. Nature nanotechnology. 2015;10(3):227.
18. Rogers JA, Lagally M, Nuzzo RG. Synthesis, assembly and applications of semiconductor nanomembranes. Nature. 2011;477(7362):45.
19. Choi DY, Kang HW, Sung HJ, et al. Annealing-free, flexible silver nanowire–polymer composite electrodes via a continuous two-step spray-coating method. Nanoscale. 2013;5(3):977-983.
20. De S, King PJ, Lotya M, et al. Flexible, transparent, conducting films of randomly stacked graphene from surfactant-stabilized, oxide-free graphene dispersions. Small. 2010;6(3):458-464.
21. Ghoshal T, Biswas S, Kar S, et al. Direct synthesis of ZnO nanowire arrays on Zn foil by a simple thermal evaporation process. Nanotechnology. 2008;19(6):065606.
22. Huo K, Hu Y, Fu J, et al. Direct and large-area growth of one-dimensional ZnO nanostructures from and on a brass substrate. The Journal of Physical Chemistry C. 2007;111(16):5876-5881.
23. Takei K, Fang H, Kumar SB, et al. Quantum Confinement Effects in Nanoscale-Thickness InAs Membranes. Nano Letters. 2011 Nov;11(11):5008-5012.
24. Dasgupta NP, Sun JW, Liu C, et al. 25th Anniversary Article: Semiconductor Nanowires Synthesis, Characterization, and Applications. Advanced Materials. 2014 Apr;26(14):2137-2184.
25. Bryllert T, Wernersson LE, Froberg LE, et al. Vertical high-mobility wrap-gated InAs nanowire transistor. Ieee Electron Device Letters. 2006 May;27(5):323-325.
26. Duan XF, Lieber CM. Laser-assisted catalytic growth of single crystal GaN nanowires. Journal of the American Chemical Society. 2000 Jan 12;122(1):188-189.
27. Hu M, Giapis KP, Goicochea JV, et al. Significant Reduction of Thermal Conductivity in Si/Ge Core-Shell Nanowires. Nano Letters. 2011 Feb;11(2):618-623.
28. Calarco R, Marso M, Richter T, et al. Size-dependent photoconductivity in MBE-grown GaN-nanowires. Nano Letters. 2005 May;5(5):981-984.
29. Choi K, Arita M, Arakawa Y. Selective-area growth of thin GaN nanowires by MOCVD. Journal of Crystal Growth. 2012 Oct 15;357:58-61.
30. Chen J, Konenkamp R. Vertical nanowire transistor in flexible polymer foil. Applied Physics Letters. 2003 Jun 30;82(26):4782-4784.
31. Calabrese G, Corfdir P, Gao GH, et al. Molecular beam epitaxy of single crystalline GaN nanowires on a flexible Ti foil. Applied Physics Letters. 2016 May 16;108(20).
32. Calleja E, Sanchez-Garcia MA, Sanchez FJ, et al. Luminescence properties and defects in GaN nanocolumns grown by molecular beam epitaxy. Physical Review B. 2000 Dec 15;62(24):16826-16834.
33. Huang HC, Kim M, Zhan X, et al. High Aspect Ratio beta-Ga2O3 Fin Arrays with Low-Interface Charge Density by Inverse Metal-Assisted Chemical Etching. ACS Nano. 2019 Jun 24.
34. Kim JD, Kim M, Chan C, et al. CMOS-Compatible Catalyst for MacEtch: Titanium Nitride-Assisted Chemical Etching in Vapor phase for High Aspect Ratio Silicon Nanostructures. ACS Appl Mater Interfaces. 2019 Jul 31;11(30):27371-27377.
35. Kim M, Yi S, Kim JD, et al. Enhanced Performance of Ge Photodiodes via Monolithic Antireflection Texturing and alpha-Ge Self-Passivation by Inverse Metal-Assisted Chemical Etching. ACS Nano. 2018 Jul 24;12(7):6748-6755.

36. Kim JD, Kim M, Kong L, et al. Self-Anchored Catalyst Interface Enables Ordered Via Array Formation from Submicrometer to Millimeter Scale for Polycrystalline and Single-Crystalline Silicon. ACS Appl Mater Interfaces. 2018 Mar 14;10(10):9116-9122.
37. Kim M, Huang HC, Kim JD, et al. Nanoscale groove textured beta-Ga2O3 by room temperature inverse metal-assisted chemical etching and photodiodes with enhanced responsivity. Applied Physics Letters. 2018 Nov 26;113(22).
38. Li X, Bohn PW. Metal-assisted chemical etching in HF/H(2)O(2) produces porous silicon. Applied Physics Letters. 2000 Oct 16;77(16):2572-2574.
39. Weisse JM, Lee CH, Kim DR, et al. Fabrication of Flexible and Vertical Silicon Nanowire Electronics. Nano Letters. 2012 Jun;12(6):3339-3343.
40. Akinwande D, Petrone N, Hone J. Two-dimensional flexible nanoelectronics. Nature Communications. 2014 Dec;5.
41. Bhimanapati GR, Lin Z, Meunier V, et al. Recent Advances in Two-Dimensional Materials beyond Graphene. Acs Nano. 2015 Dec;9(12):11509-11539.
42. Zheng Y, Yuan C, Wei S, Kim H, Yao F, Seo J.-H. Direct Growth of Two Dimensional Molybdenum Disulfide on Flexible Ceramic Substrate. Nanomaterials 2019 Oct; 9(10): 1456.
43. Liang S, Hasan MN, Seo J.-H. Direct Observation of Raman Spectra in Black Phosphorus under Uniaxial Strain Conditions. Nanomaterials 2019 April; 9(4): 566.
44. Li XQ, Lin SS, Lin X, et al. Graphene/h-BN/GaAs sandwich diode as solar cell and photodetector. Opt Express. 2016 Jan 11;24(1):134-145.
45. Splendiani A, Sun L, Zhang YB, et al. Emerging Photoluminescence in Monolayer MoS2. Nano Letters. 2010 Apr;10(4):1271-1275.
46. Xia FN, Mueller T, Lin YM, et al. Ultrafast graphene photodetector. Nat Nanotechnol. 2009 Dec;4(12):839-843.
47. Mueller T, Xia FNA, Avouris P. Graphene photodetectors for high-speed optical communications. Nat Photonics. 2010 May;4(5):297-301.
48. Urich A, Unterrainer K, Mueller T. Intrinsic Response Time of Graphene Photodetectors. Nano Letters. 2011 Jul;11(7):2804-2808.
49. Liu N, Tian H, Schwartz G, et al. Large-Area, Transparent, and Flexible Infrared Photodetector Fabricated Using P-N Junctions Formed by N-Doping Chemical Vapor Deposition Grown Graphene. Nano Letters. 2014 Jul;14(7):3702-3708.
50. Wei P, Liu N, Lee HR, et al. Tuning the Dirac Point in CVD-Grown Graphene through Solution Processed n-Type Doping with 2-(2-Methoxyphenyl)-1,3-dimethyl-2,3-dihydro-1H-benzoimidazole. Nano Letters. 2013 May;13(5):1890-1897.
51. Kim TY, Ha J, Cho K, et al. Transparent Large-Area MoS2 Phototransistors with Inkjet-Printed Components on Flexible Platforms. Acs Nano. 2017 Oct;11(10):10273-10280.
52. Rogers JA, Lagally MG, Nuzzo RG. Synthesis, assembly and applications of semiconductor nanomembranes. Nature. 2011 Sep 1;477(7362):45-53.
53. Cho M, Seo J.-H., Kim M, et al. Resonant cavity germanium photodetector via stacked single-crystalline nanomembranes. J Vac Sci Technol B. 2016 Jul;34(4).
54. Cho M, Seo J.-H., Lee J, et al. Ultra-thin distributed Bragg reflectors via stacked single-crystal silicon nanomembranes. Applied Physics Letters. 2015 May 4;106(18).
55. Cho M, Seo J.-H., Zhao DY, et al. Amorphous Si/SiO2 distributed Bragg reflectors with transfer printed single-crystalline Si nanomembranes. J Vac Sci Technol B. 2016 Jul;34(4).
56. Jung YH, Chang TH, Zhang H, et al. High-performance green flexible electronics based on biodegradable cellulose nanofibril paper. Nat Commun. 2015 May 26;6:7170.
57. Kim M, Cho SJ, Dave YJ, et al. Fabrication of Ge-on-insulator wafers by Smart-Cut (TM) with thermal management for undamaged donor Ge wafers. Semiconductor Science and Technology. 2018 Jan;33(1).
58. Kim M, Mi HY, Cho M, et al. Tunable biaxial in-plane compressive strain in a Si nanomembrane transferred on a polyimide film. Applied Physics Letters. 2015 May 25;106(21).

59. Kim M, Seo J.-H., Singisetti U, et al. Recent advances in free-standing single crystalline wide band-gap semiconductors and their applications: GaN, SiC, ZnO, beta-Ga2O3, and diamond. Journal of Materials Chemistry C. 2017 Sep 7;5(33):8338-8354.
60. Kim M, Seo J.-H., Zhao DY, et al. Transferrable single crystalline 4H-SiC nanomembranes. Journal of Materials Chemistry C. 2017 Jan 14;5(2):264-268.
61. Bruel M, Aspar B, AubertonHerve AJ. Smart-cut: A new silicon on insulator material technology based on hydrogen implantation and wafer bonding. Japanese Journal of Applied Physics Part 1-Regular Papers Short Notes & Review Papers. 1997 Mar;36(3b):1636-1641.
62. Zhang K, Jung YH, Mikael S, et al. Origami silicon optoelectronics for hemispherical electronic eye systems. Nat Commun. 2017 Nov 24;8(1):1782.
63. Zhou WD, Zhao DY, Shuai YC, et al. Progress in 2D photonic crystal Fano resonance photonics. Progress in Quantum Electronics. 2014 Jan;38(1):1-74.
64. Kim M, Liu SC, Kim TJ, et al. Light absorption enhancement in Ge nanomembrane and its optoelectronic application. Opt Express. 2016 Jul 25;24(15):16894-903.
65. Kim M, Seo J.-H., Yu ZF, et al. Flexible germanium nanomembrane metal-semiconductor-metal photodiodes. Applied Physics Letters. 2016 Aug 1;109(5).
66. Xia Z, Song H, Kim M, et al. Single-crystalline germanium nanomembrane photodetectors on foreign nanocavities. Sci Adv. 2017 Jul;3(7):e1602783.
67. Liu D, Cho SJ, Park J, et al. 226 nm AlGaN/AlN UV LEDs using p-type Si for hole injection and UV reflection. Applied Physics Letters. 2018 Jul 2;113(1).
68. Liu D, Cho SJ, Park J, et al. 229 nm UV LEDs on aluminum nitride single crystal substrates using p-type silicon for increased hole injection. Applied Physics Letters. 2018 Feb 19;112(8).
69. Liu D, Xia ZY, Cho S, et al. Cavity enhanced 1.5 mu m LED with silicon as hole injector. Proc Spie. 2016;9767.
70. Seo J.-H., Zhang K, Kim M, et al. Flexible Phototransistors Based on Single-Crystalline Silicon Nanomembranes. Advanced Optical Materials. 2016 Jan;4(1):120-125.
71. Camacho-Aguilera RE, Cai Y, Patel N, et al. An electrically pumped germanium laser. Opt Express. 2012 May 7;20(10):11316-11320.
72. Mohammad SN, Salvador AA, Morkoc H. Emerging Gallium Nitride Based Devices. P Ieee. 1995 Oct;83(10):1306-1355.
73. Park SH, Yuan G, Chen DT, et al. Wide Bandgap III-Nitride Nanomembranes for Optoelectronic Applications. Nano Letters. 2014 Aug;14(8):4293-4298.
74. Nunez CG, Vilouras A, Navaraj WT, et al. ZnO Nanowires-Based Flexible UV Photodetector System for Wearable Dosimetry. IEEE Sensors Journal. 2018;18(19):7881-7888.
75. Zhang H, Dai X, Guan N, et al. Flexible Photodiodes Based on Nitride Core/Shell p-n Junction Nanowires. ACS Applied Materials & Interfaces. 2018 Oct;8(39):26198-26206.
76. Mulazimoglu E, Coskun S, Gunoven M, et al. Silicon nanowire network metal-semiconductor-metal photodetectors. American Institute of Physics. 2013 Aug 19;103(8):83114.
77. Aksoy B, Coskun S, Kucukyildiz S, et al. Transparent, highly flexible, all nanowire network germanium photodetectors. Nanotechnology. 2012;23(32):325202.
78. Zhang S, Cai L, Wang T, et al. Fully printed flexible carbon nanotube photodetectors. Applied Physics Letters. 2017 2017/03/20;110(12):123105.
79. Pathirane MK, Wong WS. Optical and Electrical Characteristics of Hybrid ZnO Nanowire/a-Si:H Solar Cells on Flexible Substrates under Mechanical Bending. Small. 2016 2016/05/01;12(19):2554-2558.
80. Liu D, Yang D, Gao Y, et al. Flexible Near-Infrared Photovoltaic Devices Based on Plasmonic Hot-Electron Injection into Silicon Nanowire Arrays. Angewandte Chemie International Edition. 2016 2016/03/24;55(14):4577-4581.
81. Fukui T, Yoshimura M, Nakai E, et al. Position-Controlled III–V Compound Semiconductor Nanowire Solar Cells by Selective-Area Metal–Organic Vapor Phase Epitaxy. AMBIO. 2012 2012/03/01;41(2):119-124.

82. Zhang H, Dai X, Guan N, et al. Flexible Photodiodes Based on Nitride Core/Shell p–n Junction Nanowires. ACS Applied Materials & Interfaces. 2016 2016/10/05;8(39):26198-26206.
83. Dai X, Messanvi A, Zhang H, et al. Flexible Light-Emitting Diodes Based on Vertical Nitride Nanowires. Nano Letters. 2015 2015/10/14;15(10):6958-6964.
84. Guan N, Dai X, Messanvi A, et al. Flexible White Light Emitting Diodes Based on Nitride Nanowires and Nanophosphors. ACS Photonics. 2016 2016/04/20;3(4):597-603.
85. Guan N, Dai X, Zhang H, et al., editors. InGaN/GaN nanowire flexible light emitting diodes and photodetectors. 2017 19th International Conference on Transparent Optical Networks (ICTON); 2017 2-6 July 2017.
86. Yukio N, Masatsugu I, Daisuke S, et al. White light emitting diodes with super-high luminous efficacy. Journal of Physics D: Applied Physics. 2010;43(35):354002.
87. Valente J, Godde T, Zhang Y, et al. Light-Emitting GaAs Nanowires on a Flexible Substrate. Nano Letters. 2018 2018/07/11;18(7):4206-4213.
88. Li, X., Liang, R., Tao, J. et al. Flexible Light Emission Diode Arrays Made of Transferred Si Microwires-ZnO Nanofilm with Piezo-Photronic Effect Enhanced Lighting. ACS Nano. 2017;11(4):3383-3389.
89. Tatebayashi J, Ota Y, Ishida S, et al. Nanowire-quantum-dot lasers on flexible membranes. APPLIED PHYSICS EXPRESS. 2018;11(6):65002.
90. Jevtics D, Hurtado A, Guilhabert B, et al. Integration of Semiconductor Nanowire Lasers with Polymeric Waveguide Devices on a Mechanically Flexible Substrate. Nano Letters. 2017 2017/10/11;17(10):5990-5994.
91. Tiwari JN, Tiwari RN, Kim KS. Zero-dimensional, one-dimensional, two-dimensional and three-dimensional nanostructured materials for advanced electrochemical energy devices. Progress in Materials Science. 2012 2012/05/01/;57(4):724-803.
92. Kim M, Kang P, Leem J, et al. A stretchable crumpled graphene photodetector with plasmonically enhanced photoresponsivity [10.1039/C6NR09338H]. Nanoscale. 2017;9(12):4058-4065.
93. Liu N, Tian H, Schwartz G, et al. Large-Area, Transparent, and Flexible Infrared Photodetector Fabricated Using P-N Junctions Formed by N-Doping Chemical Vapor Deposition Grown Graphene. Nano Letters. 2014 2014/07/09;14(7):3702-3708.
94. Asad M, Salimian S, Sheikhi MH, et al. Flexible phototransistors based on graphene nanoribbon decorated with MoS2 nanoparticles. Sensors and Actuators, A: Physical. 2015;232:285-291.
95. Kang M-A, Kim SJ, Song W, et al. Fabrication of flexible optoelectronic devices based on MoS2/graphene hybrid patterns by a soft lithographic patterning method. Carbon. 2017 2017/05/01/;116:167-173.
96. Sun B, Shi T, Liu Z, et al. Large-area flexible photodetector based on atomically thin MoS2/graphene film. Materials & Design. 2018 2018/09/15/;154:1-7.
97. An J, Le T-SD, Lim CHJ, et al. Single-Step Selective Laser Writing of Flexible Photodetectors for Wearable Optoelectronics. Advanced Science. 2018 2018/08/01;5(8):1800496.
98. Liu Y, Liu Y, Qin S, et al. Graphene-carbon nanotube hybrid films for high-performance flexible photodetectors. Nano Research. 2017 2017/06/01;10(6):1880-1887.
99. Zheng Z, Zhang T, Yao J, et al. Flexible, transparent and ultra-broadband photodetector based on large-area WSe 2 film for wearable devices. Nanotechnology. 2016;27(22):225501.
100. Yu F, Hu M, Kang F, et al. Flexible photodetector based on large-area few-layer MoS2. Progress in Natural Science: Materials International. 2018 2018/10/01/;28(5):563-568.
101. Velusamy DB, Kim RH, Cha S, et al. Flexible transition metal dichalcogenide nanosheets for band-selective photodetection [Article]. Nature Communications. 2015 09/02/online;6:8063.
102. Zhong MZ, Huang L, Deng HX, et al. Flexible photodetectors based on phase dependent Pbl(2) single crystals. JOURNAL OF MATERIALS CHEMISTRY C. 2016;4(27).
103. Zhang J, Huang Y, Tan Z, et al. Low-Temperature Heteroepitaxy of 2D PbI2/Graphene for Large-Area Flexible Photodetectors. Advanced Materials. 2018 Sep 1;30(36):1803194.

104. Feng W, Gao F, Hu Y, et al. High-performance and flexible photodetectors based on chemical vapor deposition grown two-dimensional In 2 Se 3 nanosheets. Nanotechnology. 2018;29(44):445205.
105. Xia J, Zhao Y-X, Wang L, et al. van der Waals epitaxial two-dimensional CdSxSe(1−x) semiconductor alloys with tunable-composition and application to flexible optoelectronics [10.1039/C7NR04968D]. Nanoscale. 2017;9(36):13786-13793.
106. Chen G, Yu Y, Zheng K, et al. Fabrication of Ultrathin Bi2S3Nanosheets for High-Performance, Flexible, Visible-NIR Photodetectors. Small. 2015;11(24):2848-2855.
107. Song J, Xu L, Li J, et al. Monolayer and Few-Layer All-Inorganic Perovskites as a New Family of Two-Dimensional Semiconductors for Printable Optoelectronic Devices. Advanced Materials. 2016 2016/06/01;28(24):4861-4869.
108. Torres Alonso E, Rodrigues DP, Khetani M, et al. Graphene electronic fibres with touch-sensing and light-emitting functionalities for smart textiles. npj Flexible Electronics. 2018;2(1):1-6.
109. Das S, Gulotty R, Sumant AV, et al. All Two-Dimensional, Flexible, Transparent, and Thinnest Thin Film Transistor. Nano Letters. 2014 April;14(5):2861-2866.
110. Rogers JA, Lagally MG, Nuzzo RG. Synthesis, assembly and applications of semiconductor nanomembranes [Review Article]. Nature. 2011 08/31/online;477:45.
111. Guo Q, Fang Y, Zhang M, et al. Wrinkled Single-Crystalline Germanium Nanomembranes for Stretchable Photodetectors. IEEE Transactions on Electron Devices. 2017;64(5):1985-1990.
112. Yang W, Yang H, Qin G, et al. Large-area InP-based crystalline nanomembrane flexible photodetectors. Applied Physics Letters. 2010;96(12):121107.
113. Jung I, Xiao J, Malyarchuk V, et al. Dynamically tunable hemispherical electronic eye camera system with adjustable zoom capability. Proceedings of the National Academy of Sciences. 2011;108(5):1788.
114. Ko HC, Stoykovich MP, Song J, et al. A hemispherical electronic eye camera based on compressible silicon optoelectronics. Nature. 2008 Aug 7;454:748.
115. Sun XY, Azad F, Wang SP, et al. Low-Cost Flexible ZnO Microwires Array Ultraviolet Photodetector Embedded in PAVL Substrate. NANOSCALE RESEARCH LETTERS. 2018;13(1):1-8.
116. Swinnich E, Hasan MN, Zeng K, Dove Y, Singisetti U, Mazumder B, Seo J.-H. Flexible b-Ga2O3 Nanomembrane Schottky Barrier Diodes. Advanced Electronic Materials. 2019 March; 5(3): 1800714.
117. Lee SH, Kim SB, Moon Y-J, et al. High-Responsivity Deep-Ultraviolet-Selective Photodetectors Using Ultrathin Gallium Oxide Films. ACS Photonics. 2017 2017/11/15;4(11):2937-2943.
118. Yang J, Yu W, Pan Z, et al. Ultra-Broadband Flexible Photodetector Based on Topological Crystalline Insulator SnTe with High Responsivity. Small. 2018 2018/09/01;14(37):1802598.
119. Lee S-M, Li W, Dhar P, et al. High-Performance Flexible Nanostructured Silicon Solar Modules with Plasmonically Engineered Upconversion Medium. Advanced Energy Materials. 2015 2015/11/01;5(21):1500761.
120. Yoon J, Jo S, Chun IS, et al. GaAs photovoltaics and optoelectronics using releasable multilayer epitaxial assemblies. Nature. 2010 05/20/online;465:329.
121. Choi JH, Cho EH, Lee YS, et al. Fully Flexible GaN Light-Emitting Diodes through Nanovoid-Mediated Transfer. Advanced Optical Materials. 2014 2014/03/01;2(3):267-274.
122. Chuwongin S, Yang W, Yang H, et al., editors. Flexible crystalline InP nanomembrane LED arrays. 2010 23rd Annual Meeting of the IEEE Photonics Society; 2010 7-11 Nov. 2010.
123. Zhou W, Ma Z, Yang H, et al. Flexible photonic-crystal Fano filters based on transferred semiconductor nanomembranes. Journal of Physics D: Applied Physics. 2009;42(23):234007.
124. Menon L, Yang H, Cho SJ, et al. Transferred flexible three-color silicon membrane photodetector arrays. IEEE Photonics Journal. 2014;7(1):1-6.
125. Xiong K, Mi H, Chang TH, et al. AlGaAs/Si dual-junction tandem solar cells by epitaxial lift-off and print-transfer-assisted direct bonding. Energy Science & Engineering. 2018;6(1):47-55.